REVIEW

Substorm: view from global MHD simulation and THEMIS observation

(Center for Exploratory Research on Humanosphere, RISH, Kyoto University)

Yao YAO

Abstract

In the geospace, a disturbance phenomenon called "substorm" are frequently observed, which can cause a great impact on elements in the humanosphere, such as radiation damage and surface charging on the satellite, health risk to astronauts due to the high-latitude radiation environment, and disasters in power transmission networks. To understand the physics of the substorm should be of prime importance, which helps us (1) to avoid such disasters by forecasting, and (2) to be a breakthrough in systematic understanding of the near-Earth environment from a global perspective, because the substorm is a global phenomenon whose signatures can be traced in most regions of the geospace. Triggering mechanism of the substorm expansion onset is one of the most important issues in the substorm research, which has not yet been exactly settled, though a number of models have been advocated previously. In this paper, I will firstly review the observational discovery of the magnetosphere that is the arena of the substorm phenomena, and then make a review on the triggering mechanism of the substorm onset, finally from a viewpoint of comparison between a global MHD simulation and multiple satellites observation the triggering mechanism will be reconsidered by the formation and evolution of high-pressure region origin from the magnetic reconnection site in the middle magnetotail.

1. Introduction

Effort of human beings to start the pace on utilization of near-Earth environment began with the launch of first satellite named "Sputnik 1" on October 4, 1957. After that numerous satellites were launched for exploring the near-Earth space. On the basis of these observations, we began to understand the near-Earth environment, which is more complicated as we speculated before. The near-Earth space environment is also known as the geospace that consists of the Earth's magnetosphere, ionosphere, upper region of the atmosphere, and the interplanetary space nearby. It is difficult to understand the geospace as a single system, because each region has different spatial scale, physical properties, and characteristic dynamic variations. The geospace is not as calm and peaceful as it looks. In the geospace, a disturbance phenomenon called "substorm" can be frequently observed. The substorm is a global phenomenon, whose signatures can be traced in the generation of high-energy particles in the magnetosphere, in aurora brightening and enhancement of the electrojet current in the ionosphere, and in heating of the thermosphere. Therefore, to understand the substorm phenomena could be a breakthrough in systematic understanding of the near-Earth space environment from a global perspective.

2. Magnetosphere

In solar system, interplanetary space is the space around the sun and other planets. The physical properties of the interplanetary space are defined by that of solar wind, which is a stream of plasma at supersonic speed ~400 km/s emanating from the upper atmosphere of the sun into the interplanetary space. The Soviet satellite Luna 1 launched on January 2, 1959 provided the first ever direct observations of the solar wind that was termed by Parker[1].

The Earth's magnetic field is not a simple dipolar field, when we consider the existence of the solar wind. It prevents the solar wind plasma from directly hitting surface of the Earth. The solar wind particles are mostly deflected around the Earth's magnetic field and cannot penetrate it due to the frozen-in theorem. The boundary separating the interplanetary space and the Earth's magnetic field is called magnetopause. On September 13, 1963 "Explorer 12" made the first obvious observations of the magnetopause[2]. Dynamic pressure of the solar wind plasma controls the outer part of the Earth's magnetic field generating a cavity called magnetosphere (Figure 1). The shape of the magnetosphere is

REVIEW

very complicated, which is the direct result of the interaction between the solar wind and the Earth's magnetic field. In the dayside, the Earth's magnetic field is compressed by the solar wind dynamic pressure that is balanced by magnetic pressure of the Earth's magnetic field. However, in the nightside the magnetic field is stretched by the solar wind stream and shaped an approximation of teardrop shape with a long tail extending outward to the lunar orbit. This part of the magnetosphere is named magnetotail. The "IMP 1" satellite provided the first detailed measurements of the magnetotail at geocentric distances up to 31.4 Re in the nightside[4]. Near the deep tail (~220 Re), "ISEE 3" satellite found the magnetotail structure does not essentially change compared to the near Earth ones[5]. In the magnetotail, lobe region occupies the most volume, which is separated by plasma sheet into the northern and the southern tail lobes. The plasma sheet is a sheet-like region of denser plasma and weaker magnetic field compared to that in the lobe region. It is also a region of closed magnetic field lines around the equatorial magnetotail, whose inner edge can extend to the geosynchronous orbit at ~6.6 Re. The near-Earth plasma sheet consists of central plasma sheet and plasma sheet boundary layer. Plasma measurements obtained from the "AMPTE" satellite have brought us a statistical image of the structure and dynamics of the near-Earth plasma sheet between ~10 and ~20 Re[6]. The region from outer edge of the ionosphere to about the geosynchronous orbit is called inner magnetosphere. In the inner magnetosphere, the magnetic field is almost dipolar, which can trap the plasma particles origin from the solar wind and the ionosphere, and build the belts of energetic particles called radiation belts or Van Allan belts. It is James Van Allen who firstly discovered the existence of the radiation belt by "Explorer" satellite in the year 1958. On the other hand, up to about 4 Re the region is called plasmasphere that is occupied by the ionospheric origin low-energetic particles. Through the outer edge of the plasmasphere, electron density undergoes a sharp decrease from 10-100 cm^{-3} to 1-10 cm^{-3}. The direct observation on the plasmaspheric plasma was obtained from "OGO-5" satellite[7].

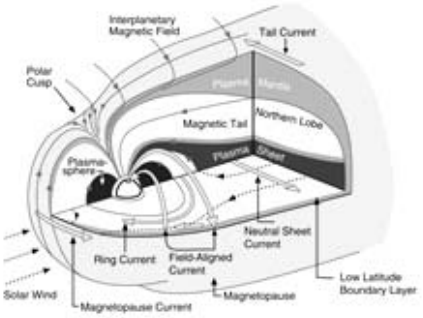

Figure 1. Schematic illustration of the Earth's magnetosphere (after De Keyser et al., 2005[3]).

3. Substorm

Aurora is one of the most beautiful phenomena mostly seen at the high latitudes of the Earth. To understand the physics of the aurora we have to introduce a transient phenomenon named "substorm". The substorm is a brief disturbance occurs in the Earth's magnetosphere. It is a significant process that can release solar wind energy stored in the magnetotail drastically into the inner magnetosphere, and the high latitude ionosphere causing sudden brightening and poleward movement of the aurora arcs. The substorm has three phases: growth phase, expansion phase, and recovery phase, which can be identified by the Auroral Electrojet (AE) index (Figure 2) that measures the global electrojet activity in the auroral zone. The interplanetary magnetic field (IMF) especially Z component is a key parameter that can affect the whole magnetosphere and ionosphere of the Earth. When the IMF B_z turns southward, the dayside reconnection will allow the solar wind particles and energy to be transferred into the magnetosphere. To our knowledge, part of the energy will be stored in the Earth's magnetotail by means of the stretched tail-like magnetic field configuration resulting in thinning of the plasma sheet. After substorm onset, the expansion phase begins and the energy will be drastically released from the magnetotail into the ionosphere, which can have a great impact on element in the humanospheric environment. The Earth-orbiting satellites are the direct sufferer mostly due to the radiation damage, or/and spacecraft charging, for example AT&T Telstar 402R geosynchronous communications satellite[8]. The high latitude radiation environments (solar energetic particles and relativistic electrons in the Earth's outer radiation belt) during a Space Particle Events (SPE) may increase a health risk to astronauts[9]. During a

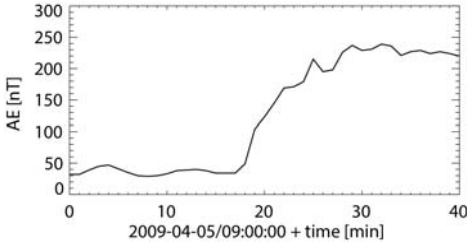

Figure 2. AE index recorded on Apr. 5, 2009.

REVIEW

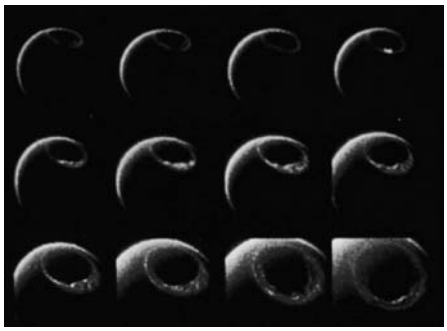

Figure 3. Consecutive false-color images of the auroral oval around the onset in a substorm on 2 April 1982 during the period 0529 through 0755 UT recorded by Dynamics Explorer 1 spacecraft (after Pfaff Jr., 2012[11]).

great storm of March 1989, a complete collapse of the Hydro-Quebec electric-power grid occurred in Canada due to sudden increase of the auroral electrojet current, and leaving nine million people without electricity for about 9 hours.

The physical process of sudden energy release associated to the substorm expansion phase is one of the most wonderful processes, which could not be found in laboratory experiments and other observable phenomena. The expansion phase begins from the substorm onset that is widely known as the time of a sudden brightening of the aurora[10] (Figure 3). However, what process triggers the onset, when and where the onset is triggered is still far from understood. Triggering mechanism of the substorm onset is one of the key issues in the substorm research. Numerous models have been proposed to explain causal relationship between the substorm associated processes in the magnetosphere, however, it is still in the debate. There are two potent candidates, one is the near-Earth neutral line (NENL) model[12] (Figure 4), in which the time sequence could be considered as, first a neutral line is formed in the near-Earth magnetotail, then magnetic reconnection begins at X_{GSM}~ −20 Re. The reconnection results in earthward bursty bulk flow (BBF)[13] that can transport mass, energy, and magnetic flux to the near-Earth region. Pileup of the magnetic flux at the inner edge of the plasma sheet causes the dipolarization, and substorm current wedges that lead to the enhancement of the auroral electrojet. The other candidate is the current disruption (CD) model[14] (Figure 5), in which the ballooning instability[15] or the cross-field current instability[16] is predicted to cause the current disruption at X_{GSM}~ −10 Re leading to the dipolarization, and finally the increase in the auroral electrojet. On the basis of these two models, two significant features can be extracted, the magnetic reconnection that occurs near the tailward edge of the thin current sheet[17], and the dipolarization that were observed by numerous satellites within a X_{GSM} range from X_{GSM}~ −6.6 to −16 Re[18, 19]. The difference between these two models is which process causes the other one. The NENL model also known as outside-in model indicates that the outmost magnetic reconnection causes the innermost dipolarization. Other triggering models are founded on the basis of these two models, for example, Pu et al.[20] proposed a synthesis of tail reconnection and current disruption model, in which the fast flow caused by the reconnection resulting in the current disruption leading to the dipolarization. In a catapult current sheet relaxation model, Machida et al.[21] suggested that enhancement of the pointing flux toward the plasma sheet center at X_{GSM}~ −12 Re causes an earthward convective flow that induces a ballooning instability or other instability causing the current disruption, the relaxation of a stretched catapult current sheet itself could develop the boundary of the stretched dipole field into the magnetic neutral line then leading to the magnetic reconnection. Current observations from multiple satellites seem to support the NENL model, that is, the magnetic reconnection in the mid-magnetotail is the trigger of the substorm onset[22].

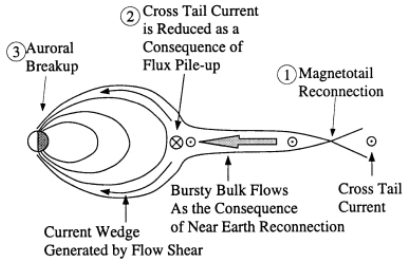

Figure 4. Near-Earth neutral line (NENL) model[34].

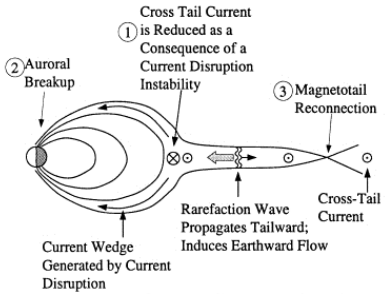

Figure 5. Current disruption (CD) model[34].

4. Evolution of high-pressure region around the substorm onset

The substorm is a global phenomenon that could couple both the magnetosphere and the ionosphere.

REVIEW

However, one-point satellite observations only reveal local features of the substorm. The current Time History of Events and Macroscale Interactions during Substorms (THEMIS) mission[23] launched on February 17, 2007 provided a unique opportunity to investigate the evolution of near-Earth plasma sheet during the substorm, which has five probes covering a wide spatial range in Sun-Earth direction. Although the THEMIS mission can provide multiple-point observations, it is still difficult to restore a whole global image of the substorm.

As the performance of computer hardware is being incredibly improved, the numerical simulation has become an important research method after theoretical research and observation. Tanaka et al.[24] developed a global magnetohydrodynamics (MHD) model that has a capability in reproducing many observable manifestations of the substorms, such as the formation of a near-Earth neutral line[12], earthward flow in the plasma sheet, stretching and dipolarization of magnetic field, sudden intensification of a westward electrojet at the auroral latitudes. In spite of the suggestion that non-MHD processes trigger a substorm[25], the global MHD simulation reasonably describes the global structure and dynamics of the magnetosphere that evolves self-consistently to satisfy mass, momentum, and energy equations.

Variation of plasma pressure in the near-Earth magnetotail is a characteristic feature around the substorm expansion onset. Statistical studies were previously carried out in the plasma sheet[6, 26, 27]. Baumjohann[28] indicated that adiabatic convective motion would lead to greatly high plasma pressure of associated flux tubes closer to the Earth. Observation in the inner magnetosphere was reported to show simultaneous pressure enhancement and magnetic depression at the onset by CRRES satellite[29]. Xing et al.[30] showed that a substantial duskward enhancement in the plasma sheet pressure gradient at 11 Re near the onset on the basis of THEMIS observations could be associated with enhanced upward field-aligned current during the late growth phase. Xing et al.[31] further found that within 2 min prior to the onset, the ion distribution function showed a substantial earthward shift, which agrees with the ion acceleration ahead of the earthward convection dipolarization front.

On the basis of a global MHD simulation, Tanaka et al.[24] pointed out that the sudden intensification of the westward auroral electrojet can be explained in terms of a substantial increase of the plasma pressure caused by the state transition (change in the force balance) in the plasma sheet. During the growth phase, about 6 minutes before the substorm expansion onset a near-Earth neutral line forms and results in the force imbalance between plasma pressure gradient force and magnetic tension force. It is always over tension in the mid-magnetotail region just before the onset, since the reduction of the pressure gradient force. The over tension state brings out earthward tension force that can accelerate the particles and generate earthward fast flow. The convergence of the fast flow contributes to the pressure enhancement that leads to the generation of high-pressure region (HPR). In other words, the plasma is squeezed in the near-Earth plasma sheet resulting in the formation of the HPR. It can also be said that the plasma implodes earthward. As a consequence, the HPR moves earthward, and reaches the inner region from X_{GSM}= −6 to −8 Re within 3 or 4 min before the onset. The generation of the HPR causes diamagnetic current that can result in an intensification of the Region 2 field-aligned currents, together with the Region 1 currents on the nightside. Then, auroral electrojets are intensified in the polar ionosphere on the nightside, which is regarded as a manifestation of the substorm onset. After the onset, the region where the plasma is squeezed spreads tailward. As a consequence, the HPR retreats tailward. From previous

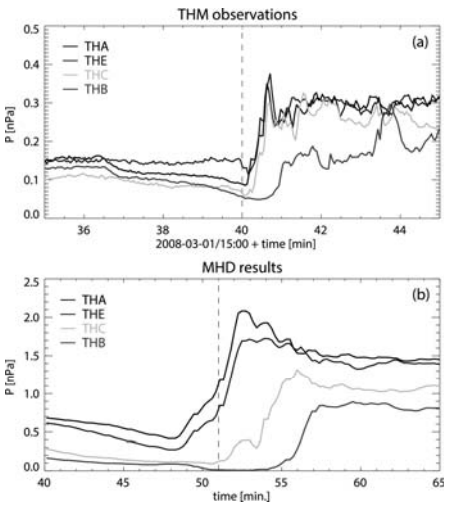

Figure 6. Comparison of plasma pressure between (a) THEMIS observations and (b) MHD simulation (after Yao et al., 2015[32]).

REVIEW

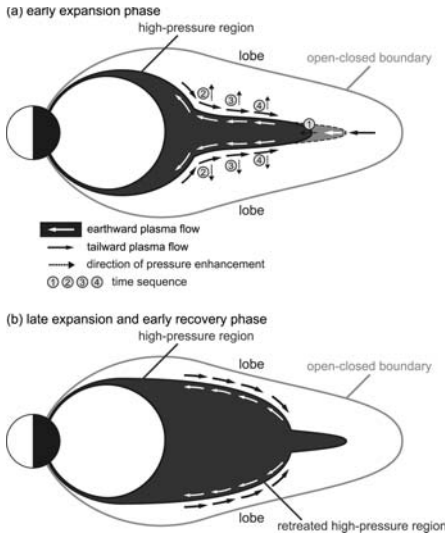

Figure 7. Schematic diagram illustrating the processes resulting in the pressure enhancement in the noon-midnight (Y_{GSM}= 0 Re) meridinoal plane (after Yao et al., 2015[32]).

studies, the evolution of the HPR in the near-Earth plasma sheet has not been clear identified, though the importance of the HPR has been indicated by Tanaka et al.[24].

During a substorm event on 1 March 2008, four THEMIS probes aligned along the Sun-Earth line, and observed a sudden pressure enhancement (SPE) from inner most probe to outer ones, which implies tailward retreat of the high-pressure region. By visual inspection, Yao et al.[32] determined the coincident position of the THEMIS probes in the MHD domain. It is found that the simulation results can reproduce the similar tailward retreat of the high-pressure region at approximate positions of the THEMIS probes in the simulation domain (Figure 6). The results of the simulation also show that at off-equator (Z_{GSM}= −1.5 Re) only the tailward retreat of the SPE can be seen in the presented case. However, at the equator there is an earthward propagation of the SPE seen firstly before the substorm onset. From viewpoint of the force balance, the tailward retreat of the SPE could be explained by the propagation of high-pressure region in $-Z_{GSM}$ direction, and from the inner to the outer along $-X_{GSM}$. The combination of the convergence of the plasma flow (velocity divergence along Z_{GSM} axis) and the pressure gradient force account for the propagation of the HPR along $-Z_{GSM}$. This process is illustrated in Figure 7.

In an isolated substorm event occurred on 5 April 2009, the earthward implosion of the HPR before the substorm onset as predicted by the global MHD simulation was identified[33] which was not identified in the study reported by Yao et al.[32]. It is found that there are two peaks of the ion pressure observed by the THEMIS probes located at X_{GSM}~ −11 Re near the equatorial plane. The first peak took place just before the substorm onset, and the second one took place just after the onset. The duration of the two pressure peaks is shorter in the inner region than that in the outer region. This is consistent with "V" structure (Figure 8) of the plasma pressure in a distance-time diagram shown from the MHD simulation. These results may provide observational evidence of the sequence of the substorm as predicted by the MHD simulation[24]. The convergence of the plasma flow caused by the change in the force balance (state transition in the plasma sheet) plays an important role in the enhancement of the plasma pressure around the substorm onset.

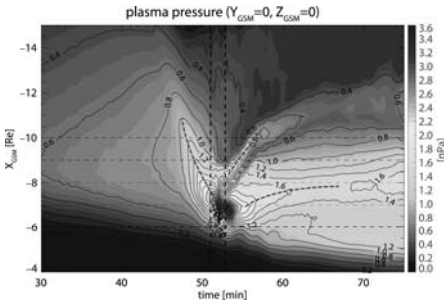

Figure 8. Temporal variation of simulated plasma pressure as a function of X_{GSM} in the equatorial plane (Y_{GSM}= 0 and Z_{GSM}= 0 Re) (after Yao et al., 2015[33]).

5. Summary

Numerical simulation has been developed into an important way after traditional theoretical research and observation. In the magnetospheric substorm study, the MHD simulation[24] gradually shows its power in understanding the physics of the substorm from a global view. Some substorm signatures have been reproduced by the MHD simulation, at the same time some significant manifestations seen from the

MHD simulation have also been identified by observational evidences.

Although the MHD simulation did not exactly simulate the substorm events reported by Yao et al.[32, 33], the simulation results seems to well reproduce what observed by the THEMIS probes. Therefore, we might believe that the MHD simulation could show us the common features of the substorm, which does not change for different substorm events. To know the whole process of the substorm in the magnetosphere-ionosphere system may help us further understanding its important impact on the region below the ionosphere, which is the core region of the humanosphere.

References

[1] Parker, E. N., "Cosmic-Ray modulation by solar wind", Phys. Rev., Vol 110, No. 6, 1445–1449, 1958.

[2] Cahill, L. J. and P. G. Amazeen, "The Boundary of the Geomagnetic Field", J. Geophys. Res., Vol 68, 1835–, 1963.

[3] De Keyser, J., et al., "Magnetopause and Boundary Layer", Space Sci. Rev., Vol. 118, Issue 1-4, 231–320, doi:10.1007/s11214-005-3834-1, 2005.

[4] Ness, N. F., "The Earth's magnetic tail", J. Geophys. Res., Vol. 70, No. 13, 2989–3005, 1965.

[5] Slavin, J. A., et al., "Average configuration of the distant (< 220 Re) magnetotail: Initial ISEE-3 magnetic field results", Geophys. Res. Lett., Vol. 10, Issue 10, 973–976, 1983.

[6] Baumjohann, W., G. Paschmann, and C. A. Cattell, "Average plasma properties in the central plasma sheet", J. Geophys. Res., Vol. 94(A6), 6597–6606, 1989.

[7] Chappell et al., "A study of the influence of magnetic activity on the location of the plasmapause as measured by OGO 5", J. Geophys. Res., Vol. 75, No. 1, 50–56, 1970.

[8] Lanzerotti, L. J., et al., Studies of spacecraft charging on a geosynchronous telecommunication satellite, Adv. Space Res., Vol 22, No. 1, 79–82, 1998.

[9] Turner, R., "Solar particle events from a risk management perspective", IEEE Tran. On Plasma Sci., Vol. 28, No. 6, 2103-2113, 2000.

[10] Akasofu, S.-I., "The development of the auroral substorm", Planet. Space Sci., Vol. 12, 273–282, 1964.

[11] Pfaff Jr., R. F., "The near-Earth plasma environment", Space Sci. Rev., Vol. 168, 23–112, 2012.

[12] Baker, D. N., T. I. Pulkkinen, V. Angelopoulos, W. Baumjohann, R. L. McPherron (1996), "Neutral line model of substorms: Past results and present view", J. Geophys. Res., Vol. 101, 12975-13010, 1996.

[13] Angelopoulos, V., et al., "Bursty bulk flows in the inner central plasma sheet", J. Geophys. Res., Vol. 97(A4), 4027–4039, 1992.

[14] Lui, A. T. Y., "Current disruption in the Earth's magnetosphere: Observations and models", J. Geophys. Res., Vol. 101(A6), 13067–13088, 1996.

[15] Roux, A., et al., "Plasma sheet instability related to the westward traveling surge", J. Geophys. Res., Vol 96(A10), 17697–17714, 1991.

[16] Lui, A. T. Y., C.-L. Chang, A. Mankofsky, H.-K. Wong, and D. Winske, "A cross-field current instability for substorm expansions", J. Geophys. Res., Vol. 96(A7), 11389–11401, 1991.

[17] Miyashita, Y., et al., Difference in magnetotail variations between intense and weak substorms, J. Geophys. Res., Vol. 109, A11205, 2004.

[18] Baumjohann, W., et al., "Substorm dipolarization and recovery", J. Geophys. Res., Vol. 104(A11), 24995–25000, 1999.

[19] Miyashita, Y., et al., “A state-of-the-art picture of substorm-associated evolution of the near-Earth magnetotail obtained from superposed epoch analysis”, J. Geophys. Res., Vol. 114, A01211, 2009.

[20] Pu, Z. Y., et al., “Ballooning instability in the presence of a plasma flow: A synthesis of tail reconnection and current disruption models for the initiation of substorms”, J. Geophys. Res., Vol. 104(A5), 10235–10248, 1999.

[21] Machida, S., et al., “Statistical visualization of the Earth's magnetotail and the implied mechanism of substorm triggering based on superposed-epoch analysis of THEMIS data”, Ann. Geophys., Vol. 32, 99-111, 2014.

[22] Angelopoulos, V., et al., “Tail reconnection triggering substorm onset”, Science, Vol. 321, 931–935, 2008.

[23] Angelopoulos, V., “The THEMIS mission”, Space Sci. Rev., 141(1–4), 5–34, 2008.

[24] Tanaka, T., et al., “Substorm convection and current system deduced from the global simulation”, J. Geophys. Res., 115, A05220, 2010.

[25] Lui, A. T. Y., et al., “Near-Earth dipolarization: Evidence for a non-MHD process”, Geophys. Res. Lett., Vol. 26, 2905–2908, 1999.

[26] Baumjohann, W., G. Paschmann, T. Nagai, H. Lühr, “Superposed Epoch Analysis of the Substorm Plasma Sheet”, J. Geophys. Res., Vol. 96, 11605–11608, 1991.

[27] Wang, Chih-Ping, Larry R. Lyons, Margaret W. Chen, Richard A. Wolf, “Modeling the quiet time inner plasma sheet protons”, J. Geophys. Res., 106, 6161–6178, 2001.

[28] Baumjohann, W., “Modes of convection in the magnetotail”, Phys. Plasma, Vol. 9(9), 3665–3667, 2002.

[29] Sergeev, V. A., et al., “Event Study of deep energetic particle injections during substorm”, J. Geophys. Res., Vol. 103, 9217–9234, 1998.

[30] Xing, X., et al., “Near-Earth plasma sheet azimuthal pressure gradient and associated auroral development soon before substorm onset”, J. Geophys. Res., Vol. 116, A07204, 2011.

[31] Xing, X., et al., “On the formation of pre-onset azimuthal pressure gradient in the near-Earth plasma sheet”, J. Geophys. Res., Vol. 117, A08224, 2012.

[32] Yao, Y., Y. Ebihara, and T. Tanaka, “Sudden pressure enhancement and tailward retreat in the near-Earth plasma sheet: THEMIS observation and MHD simulation”, J. Geophys. Res. Space Physics, Vol. 120, 201–211, 2015.

[33] Yao, Y., Y. Ebihara, and T. Tanaka, "Formation and evolution of high-plasma-pressure region in the near-Earth plasma sheet: Precursor and postcursor of substorm expansion onset", J. Geophys. Res. Space Physics, Vol. 120, 6427–6435, doi:10.1002/2015JA021187, 2015.

[34] http://www.igep.tu-bs.de/forschung/weltraumphysik/projekte/themis/wissziel_en.html.

REVIEW

The cases of Bostrichidae infestation in Japan

(Center for Exploratory Research on Humanosphere, RISH, Kyoto University)

Lee-Jin Bong

Abstract

The infestation cases from 1980 – 2014 were obtained from Japan pest control companies. A total of 52 cases were reported from the past 34 years, concentrated mostly in Chubu and Kinki regions. Low intensity of Bostrichidae infestation was recorded in the Northern of Japan. Of 52 cases, approximately 65% were caused by *Lyctus* species, with 23 cases by *L. brunneus*, followed by 11 cases by *L. africanus*. The infestations by other Bostrichidae e.g. *H. hamatipennis*, *D. minutus*, *M. rugicollis*, *L. sinensis*, and *L. linearis* were comparatively low, although these Bostrichidae were also found to have become established in Japan.

Bostrichidae, powder-post beetles, are among the most destructive wood attacking beetles that are of economic importance in forestry and lumber industries. It comprises at least 550 described species in 99 genera worldwide (Ivie 2002). Most bostrichids are not host-specific and attack wide range of timber. Both the adults and larvae cause extensive damage to timber by boring into the timber, feeding on the woody tissues of the timber for development, and reducing the wood into fine flour-like dust known as frass. The presence of their attacks in the timber is often undetectable until the appearance of hole or frass been produced.

Of 550 identified bostrichids species distributed worldwide, 16 species are currently found in Japan. These bostrichidae were not origin from japan. They were introduced into Japan by imported furniture or wood from mostly Southeast Asia. However, only 8 of them were found to have become established in

Appendix 1. Example of the survey form sending to pest control companies

調査用紙：過去からの変遷も重要な調査項目となりますので、できるだけ多くのデータのご記入をお願いいたします。

複数の枚数となる場合は、本用紙をコピーしてお使い下さい。

年	加害昆虫種（別紙をご参照下さい）	被害発生場所（市町村レベルまでお答えいただければ助かります）	物件数	被害を受けた家具/部材	被害を受けた樹種	被害を受けた部材の原産地および加工地	被害の状況
例：2013	例：La	例：京都市	9	例：机、椅子、木製おもちゃ、床、壁など	例：ラワン材	例：マレーシア	例：新築住宅の壁下地材（南洋材合板）より成虫が脱出
~~2015~~							
2012 ～ 2014	La	和歌山市	1	壁、フロア	ラワン材		新築後 7年めに 1F・2Fの フロア 1F・2Fの クロス 壁(コンパネ)より成虫が脱出

Japan: *Heterobostrychus hamatipennis* Lesne, *Rhizopertha dominica* (Fabricius), *Dinoderus minutus* Fabricius, *Lyctus africanus* Lesne, *Minthea rugicollis* (Walker), *L. sinensis* Lesne, *L. linearis* (Goeze), and *l. brunneus* (Stephens) (Mito and Uesugi 2004). These species have become invasive that brought adverse

REVIEW

effect to several economic industries in Japan, especially forestry and lumber industries.

Up to date, the intensity of Bostrichidae infestation in Japan is unknown. So, the infestation cases from 1980 – 2014 were obtained from Japan pest control companies. These cases were based on the complaints from the public to the companies. Of 700 companies, we only obtained the feedbacks from 20 companies. The information from the feedbacks were as stated in Appendix 1.

From the feedbacks, a total of 52 cases were reported from the past 34 years, concentrated mostly in Chubu and Kinki regions (Figure 1). Of the 52 cases, approximately 65% were caused by *Lyctus* species, with 23 cases by *L. brunneus*, followed by 11 cases by *L. africanus*. In Nigata and Wakayama, 8 cases caused by *L. brunneus* and *L. africanus*, respectively, were reported. This report was based on the feedbacks from the 20 companies out of 700 companies. So, the cases is expected to be greater than the presently reported cases. From Figure 1, it also showed low intensity of Bostrichidae infestation in the Northern of Japan. Environmental factor, e.g. cool weather might play a role for the low infestation. For example, in Hokkaido, the weather was relatively cool throughout the year, with the temperature not exceeding 25℃ in the summer. The cool weather is not favorable for Bostrichidae to establish their population as mentioned by Sutherst (1991), and Robinet and Roques (2010).

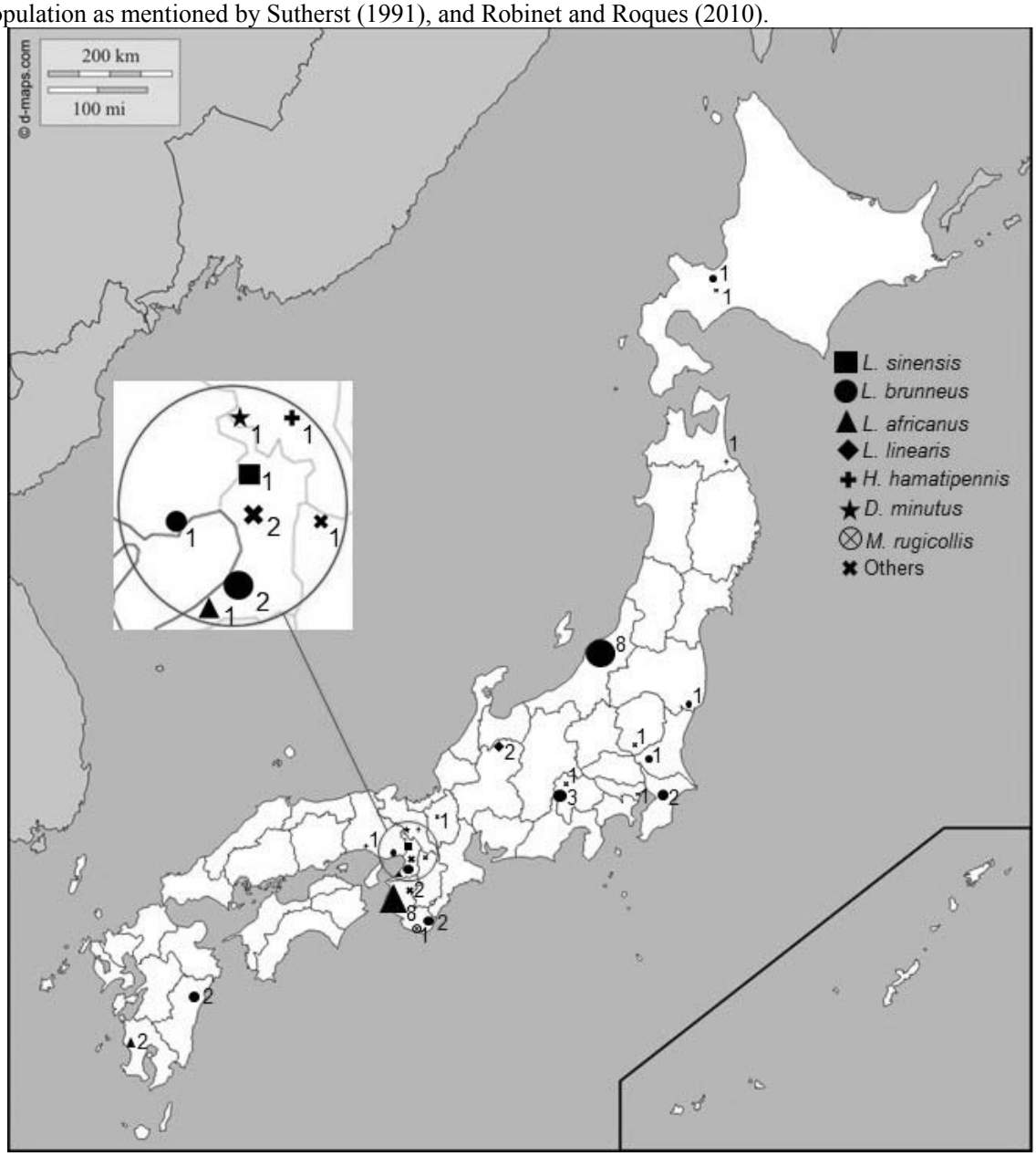

Figure 1. Reported bostrychidae infestation in Japan from 1984 to 2014

REVIEW

Both *L. brunneus* and *L. africanus* were found to infest wooden objects of the houses (Figure 2). As wooden structure buildings are very common in Japan. So, it is not uncommon to see the beetles infest the floors, ceilings, and walls, especially on the plywood and veneer. It was reported that the infestation by the beetles not only restricted to softwood, but they also infested plywood or veneer made of hardwood (Figure 3).

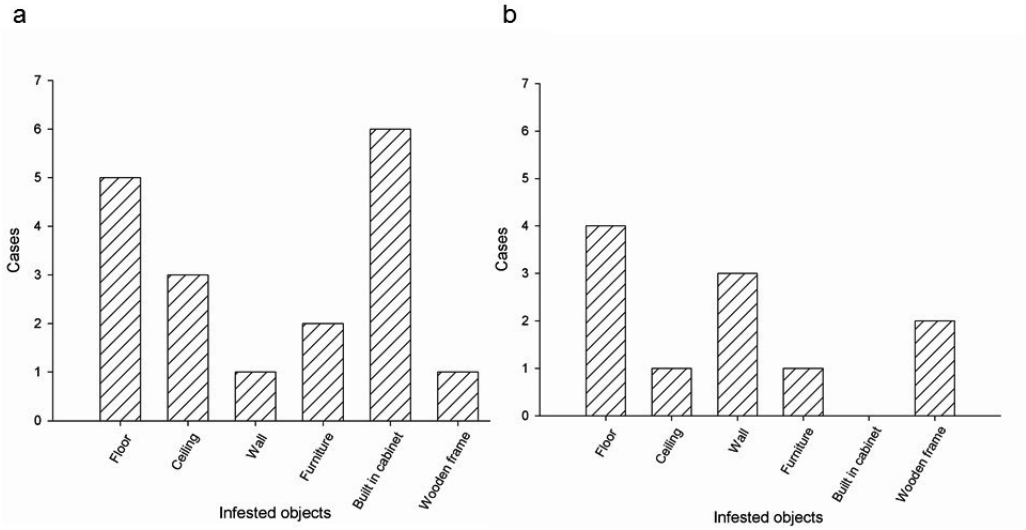

Figure 2. Housing objects infested by a) *L. brunneus* and b) *L. africanus*

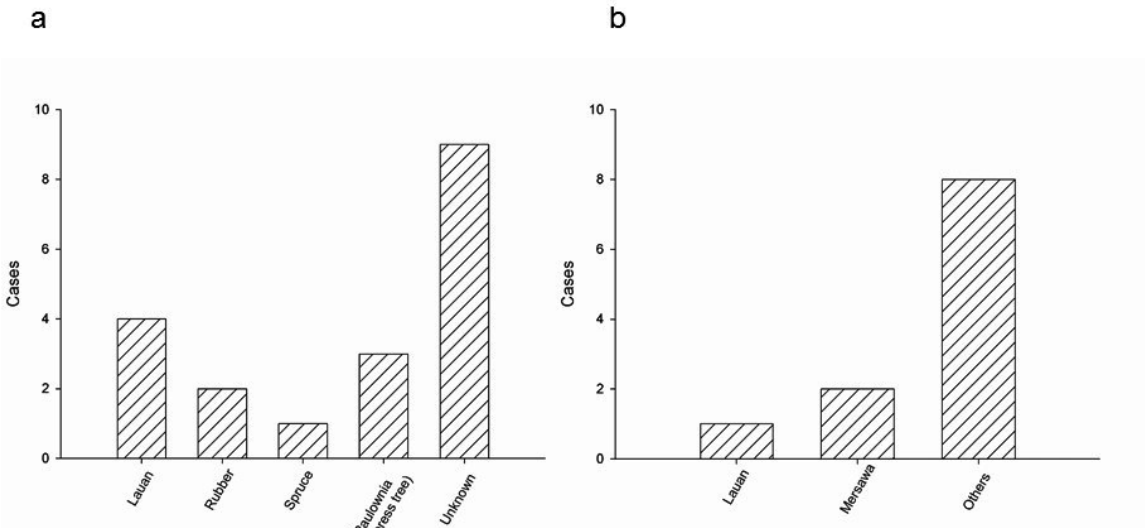

Figure 3. Types of woods infested by a) *L. brunneus* and b) *L. africanus*

The infestations by other Bostrichidae e.g. *H. hamatipennis*, *D. minutus*, *M. rugicollis*, *L. sinensis*, and *L. linearis* were comparatively low, although these Bostrichidae were also found to have become established in Japan (Figure 1). Similar to *L. brunneus* and *L. africanus*, these Bostrichidae were reported to infest wooden objects of the houses (Table 1).

REVIEW

Table 1. Types of objects infested by wood attacking beetles

Species	Infested objects
L. linearis	Furniture (desk, shelf), wall
L. sinensis	Furniture (bed)
H. hamatipennis	Floor, ceiling, decorative wooden objects
D. minutus	-
M. rugicollis	Ceiling
Others	Wall, staircase

Recently, *H. aequalis* (Waterhouse) (Figure 4), another invasive alien species has caught the public's attention in Japan. This species was introduced and intercepted in Japan from imported timber and timber products, but establishment of this species in Japan has not yet been recorded. This beetle was first found in seasoned wood of imported lauan timber in Naha, Okinawa (Nobuchi 1986). Then, another 2 cases were reported in 1994 and 1995 (Kawakami 1996). Although there were no infestation cases reported in our study (Figure 1), the occurrence of this species is increasing and gradually becoming pest in Japan (pers. comm.).

The development of Bostrichidaae is confined in the wood. So, early detection of the presence of these beetle is impossible until holes and frass have been produced, which indicates serious damage on the wood. So, it is always a challenge to forestry and lumber industries to carry out remedial action on the infested wood to eradicate the beetle. To early detect the presence of Bostrichidae, pheromone-based trap is one approach. Thus, pheromone study of these Bostrichidae is in dire need in effort to develop sustainable pest management in ways that minimize economic, health, and environmental risks in forestry and lumber industries.

Acknowledgements

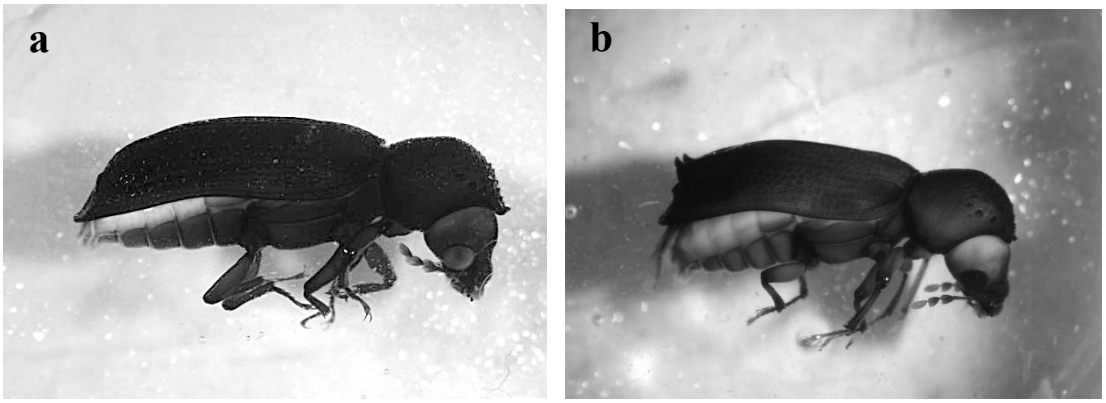

Figure 4. The (a) female, and (b) male of *H. aequalis*

We thank RISH for the support of this survey study; the pest control companies for providing data about the complaints of Bostrichidae infestation in Japan; Izumi Fujimoto for the translation, and all the lab. Members for the preparations of the survey forms.

References

[1] **Ivie, M. A. 2002.** Bostrichidae Latreille 1802, pp. 233-244. *In* R. H. Arnett, M. C. Thomas, P. E. Skelley and J. H. Frank [eds.], American beetles: polyphaga: Scarabaeoidea through Curculionoidea. CRS Press, Boca Raton, Florida.

[2] **Kawakami, Y. 1996.** Heterobostrychus aequalis (Waterhouse) (Coleoptera: Bostrychidae) further found in Japan. 家屋害虫 18: 17-20.

REVIEW

[3] **Mito, T., and T. Uesugi. 2004.** Invasive alien species in Japan: the status quo and the new regulation for prevention of their adverse effects. Global Environment Research 8: 171-191.

[4] **Nobuchi, A. 1986.** Two new discovered species of Bostrychidae (Coleoptera) from Japan. 木材保存 12: 237-241.

[5] **Robinet, C. and A. Roques. 2010.** Direct impacts of recent climate warming on isect populations. Integrative Zoology 5: 132-142.

[6] **Sutherst, R. W. 1991.** Predicting the survival of immigrant insect pest in new environments. Butterworth-Heinemann Ltd., Oxford, UK.

RECENT RESEARCH ACTIVITIES

CESEC (Cellulose Synthesizing *E. coli*): cellulose synthase reconstituted in *E. coli*

(Laboratory of Biomass Morphogenesis and Information, RISH, Kyoto University)

Tomoya Imai

Cellulose, an abundant biopolymer on Earth, has a simple molecular structure of β1→4–glucan. In the native cellulose, these molecules are packed and selectively crystallized into "cellulose I" with a slender fiber called "microfibril". Not only polymerization but also assembly of long cellulose molecules to a microfibril during the biosynthesis is the reaction operated by cellulose synthase, a hetero-subunit enzyme complex. To understand the mechanism of enzymatic reaction in general, it is extraordinary important to use recombinant protein. However only a few studies until now have reported the cellulose synthesis with recombinant cellulose synthase, and then our understanding cellulose biosynthesis is still poor owing to the lack of evidences. We then aimed to establish an easy platform for analyzing recombinant cellulose synthase, by heterogously overexpressing cellulose synthase in an experimental bacterium *Escherichia coli*.

Cellulose synthase expressed in *E. coli* produced cellulose out of *E. coli*

CesA and CesB protein of *Gluconacetobacter xylinus*, the minimally required subunits for the activity, were expressed together with diguanylate cyclase (DGC, c-di-GMP synthase) in *E. coli* by using a conventional expression vector; c-di-GMP is the activator of bacterial cellulose synthase. The *E. coli* cells were cultured, and the synthesized cellulose was analyzed by colorimetric quantification, electron microscopy, FTIR, and X-ray diffraction. The detail is described elsewhere [1].

Colorimetric quantification indicated, as previously shown, that CesA, CesB, and c-di-GMP are required for cellulose synthesis. Electron microscopy before chemically washing out *E. coli* cells showed thin fibers outside the cell (Figure 1A), which were removed by cellulase treatment. Noticeably, such a fiber structure was not found after the chemical washing, globular aggregations being found instead (Figure 1B). Electron diffraction demonstrated that this globular structure is "cellulose II" (a non-native structure of cellulose), and it was also supported by FTIR and X-ray diffraction. Given that the chemical treatment for washing was too mild to convert cellulose I to cellulose II, the fiber structure shown in Figure 1A was not cellulose I microfibril but a highly unstable unprecedented structure of cellulose which is the direct product synthesized by recombinant cellulose synthase expressed in *E. coli*.

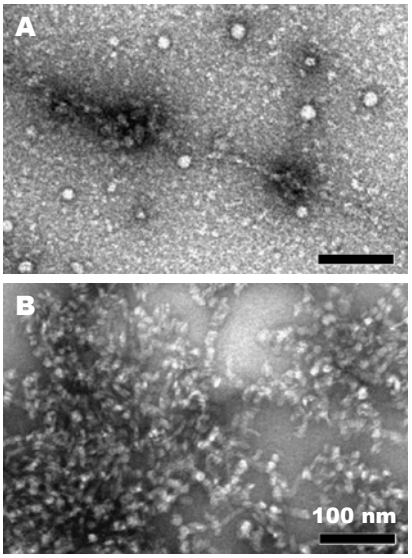

Figure 1. Electron micrographs of negatively stained cellulose synthesized in *E. coli*, before (A) and after (B) chemical washing

We thus successfully reconstituted cellulose synthase in *E. coli*, despite the disability to produce the native structure of cellulose. We designated this platform as "CESEC (Cellulose-synthesizing *E. coli*)", and are now trying to find the factor(s) essential for the production of cellulose I microfibril in CESEC. Notwithstanding CESEC will be a useful tool for analyzing cellulose synthase in the molecular level for example with rational design of enzyme by site-directed mutagenesis as well as random mutagenesis.

Acknowledgements

This is a corroborative work with Ms. Sun, S.-j., Dr. Horikawa, Y., Dr. Wada, M., and Prof. Sugiyama, J. A part of analyzes was made with DASH/FBAS in CER/RISH and ADAM in RISH, Kyoto University.

Reference

[1] Imai, T., Sun, S.-j., Horikawa, Y., Wada, M., Sugiyama, J., "Functional reconstitution of cellulose synthase in *E. coli*", *Biomacromolecules*, 14, 4206-4213, 2014

RECENT RESEARCH ACTIVITIES

Lignin–polysaccharide network analysis in wood lignocellulose

(Laboratory of Biomass conversion, RISH, Kyoto University)

Hiroshi Nishimura and Takashi Watanabe

Lignocellulosic biomass is promising resource with great potential for sustainable production of energy and various chemical products through its degradation. In recent years, the global warming and environmental pollution caused by excessive use of fossil fuels became serious problem for our environment. Hence, the utilization of woody biomass as energy and chemical resources is an urgent task for our sustaining life. Wood is essentially composed of cellulose, hemicelluloses and lignin. In the cell wall, these three polymers link together and form complexes. In a process of woody biomass conversion, separation of carbohydrate and lignin is a crucial step. In this study, we analyzed chemical structure of lignin-carbohydrate (LC) linkages in softwood using nuclear magnetic resonance (NMR) spectroscopy. In plant cell walls, lignin is covalently bound to carbohydrate, mainly hemicelluloses, to form lignin-carbohydrate complexes (LCCs).[1] The frequency of LC linkages is very limited, but these linkages are crucially important in the separation and conversion of renewable wood and plant resources. However, the structure of linkages between lignin and carbohydrate is not fully understood. Major LC linkages are known as benzyl ester and benzyl ether bonds.[1] Recently, LC bonds of phenyl glycoside and γ-ester are reported by using NMR analysis.[2] To determine the LC structure unequivocally, we studied the chemical structure of LC linkages in natural wood using 2D-NMR based on not only direct correlations but also long-range correlations. As a result of ^{1}H-^{13}C heteronuclear single quantum correlation (HSQC) NMR spectroscopy, direct correction signals were observed and tentatively assigned as those from a benzyl ether LC bond. Because the frequency of LC bonds in the extracted LCCs is still too small to detect the long-range correlation signals, the purification and the concentration processes of the LC bonds were very effective to detect the correlation signals. We developed the method to separate LC fractions and analyzed the LC bond by long-range correlated 2D-NMR. These procedures and analyses would provide fundamental information on the wood chemistry. Further studies are needed to elucidate the entire molecular structure of LCCs.

References

[1] Koshijima, T., Watanabe, T., (2003) T. Association between Lignin and Carbohydrates in Wood and Other Plant Tissues; Springer: Berlin, Germany.

[2] Balakshin, M., Capanema, E., Gracz, H., Chang, H.-m., Jameel, H., (2011) Quantification of lignin-carbohydrate linkages with high-resolution NMR spectroscopy, Planta, 233, 1097-1110.

RECENT RESEARCH ACTIVITIES

Studies on Structure, Biosynthesis, and Metabolic Engineering of Grass Lignocelluloses for Biorefinery Systems

(Laboratory of Metabolic Science of Forest Plants and Microorganisms, RISH, Kyoto University)

Toshiaki Umezawa, Yuki Tobimatsu, Shiro Suzuki, Masaomi Yamamura

It is becoming increasingly important to establish a sustainable society that depends on renewable resources. As lignocellulosic biomass is the most abundant renewable and carbon-neutral resource on earth, their better utilization and more efficient production are key strategies for realizing the goal. Among a wide variety of potential feedstock for bioenergy and bioproduct supply, large-sized grass species have attracted particular attention because of their superior growth and adaptability. In this context, we have been interested in understanding structure and biosynthesis of lignocellulose in a variety of large-sized grass species, such as *Erianthus* spp. and *Sorghum* spp. Our research also focuses on gaining basic knowledge for future metabolic engineering and breeding to improve production and utilization properties of grass lignocelluloses. For this purpose, we use rice as a model plant. Our program typically integrates many research ideas and approaches based on chemistry, biochemistry, molecular biology, and metabolomics. Some key elements of our recent research program are described below.

Lignin is a major component of secondary cell walls, and is typically considered to be an obstacle in many agro-industrial processes for polysaccharide-oriented biomass utilizations such as chemical pulping and biofuel productions. Meanwhile, lignins are abundant aromatic biopolymers showing potential as a feedstock for bio-based aromatic fine chemicals. Moreover, lignins have higher calorific values than those of plant polysaccharides, and therefore a high lignin content lignocellulose could be a good fuel in direct combustion. In this context, we and collaborators generated various rice transgenic lines in which specific genes functioning in lignin biosynthetic pathway were downregulated and/or upregulated. Until now, we have identified several transgenic lines showing intriguing lignin phenotypes, which are potentially useful for enhanced biomass utilizations [1,2]. In addition, we have elucidated previously undescribed biochemical features of several enzymes involved in lignin biosynthetic pathway as well as related transcription factors involved in secondary wall formation in rice [1,3].

Large-sized grass species such as *Erianthus* spp. and *Sorghum* spp. have been drawn attention as potential feedstock for future biorefineries. However, structural details of grass lignocelluloses and their relationship with utilization properties are not sufficiently understood. Therefore, using highly sensitive wet-chemical methods and state-of-the-art spectroscopic methods, we have elucidated detailed structures of lignocelluloses from different organs and tissues isolated from *Erianthus arundinaceus*. One of our key findings was that the saccharification efficiencies are considerably different among the different organs and tissues. Our data suggest that both structures and assembly of lignin and polysaccharide components are key factors affecting the properties of grass lignocellulosic materials [4].

References

[1] Koshiba T, Hirose N, Mukai M, Yamamura M, Hattori T, Suzuki S, Sakamoto M, Umezawa T (2013) Characterization of 5-hydroxyconiferaldehyde *O*-methyltransferase in *Oryza sativa*. *Plant Biotechnol.* **30**, 157–167

[2] Koshiba T, Murakami S, Hattori T, Mukai M, Takahashi A, Miyao A, Hirochika H, Suzuki S, Sakamoto M, Umezawa T (2013) *CAD2* deficiency causes both brown midrib and gold hull and internode phenotypes in *Oryza sativa* L. cv. Nipponbare. *Plant Biotechnol.* **30**, 157–167.

[3] Noda S, Koshiba T, Hattori T, Yamaguchi M, Suzuki S, Umezawa T (2015) The expression of a rice secondary wall-specific cellulose synthase gene, *OsCesA7*, is directly regulated by a rice transcription factor, OsMYB58/63. *Planta*, in press (DOI: 10.1007/s00425-015-2343-z).

[4] Yamamura M, Noda S, Hattori T, Shino A, Kikuchi J, Takabe K, Tagane S, Gau M, Uwatoko N, Mii M, Suzuki S, Shibata D, Umezawa T (2013) Characterization of lignocellulose of *Erianthus arundinaceus* in relation to enzymatic saccharification efficiency. *Plant Biotechnol.* **30**, 25–35.

RECENT RESEARCH ACTIVITIES

Changes in rhizosphere bacterial communities of soybean grown in the field

(Laboratory of Plant Gene Expression, RISH, Kyoto University)

Akifumi Sugiyama and Kazufumi Yazaki

The rhizosphere is the small zone of soil under influence of roots, where interaction between plants and millions of microbes occur. Rhizosphere microbes were shown to have an intense activity and suggested to be important for plant growth and health. Arbuscular mycorrhizal fungi and rhizobia provide phosphorous and nitrogen, respectively. In addition, microbes called plant-growth-promoting rhizobacteria (PGPR) were shown to exert both direct and indirect influences on plant. Recently, these rhizosphere microbes are regarded as important components for sustainable agriculture, and for sustainable humanosphere. Plants provide a platform and nutrients mainly as root exudates, which account for 10 to 40% of photosynthates and have been shown to accommodate rhizosphere microbes. Because rhizosphere microbial communities are important in growth and performance, they have been extensively studied using both culture-dependent and culture-independent methods. Recent advances in the sequencing methods provided tools for in-depth analyses of rhizosphere microbial communities. However, despite the increases in community-based analyses of rhizosphere bacterial communities, it still remains unclear how plant and bacteria communicate to form communities in the rhizosphere.

Legume plants include important crop such as soybean, which supplies nutrients rich in protein and oil for human, thus constituting an important part in humanosphere. Despite the large number of studies analyzing the legume-rhizobia and legume-arbuscular mycorrhizal fungi interactions, the mechanisms underlying legume plant interactions with vast varieties soil microbes during the growth in the field remain elusive. To expand the understanding of legume-microbe interactions in the field, and to obtain basic information on the rhizosphere bacterial communities of soybean for further research, bacterial communities of rhizospheres and bulk soils were analyzed during the entire soybean growth in a field in Kyoto Prefecture, Japan. The physiological properties of the bacterial communities were analyzed by community-level BioLog substrate utilization assays. In addition, the 16S ribosomal RNA (rRNA) gene, which is the most important target in the study of bacteria, was analyzed by PCR amplicon pyrosequencing. The results of this study suggest that plant growth could affect the composition of rhizosphere bacterial communities in addition to the seasonal effects.

Physiological properties of the bacterial communities of soybean were analyzed by BioLog Eco Plates which is a community-level substrate utilization assay, and the composition of the rhizosphere bacterial communities was assessed by gene pyrosequencing using GS Junior. In the BioLog assay higher metabolic capabilities were observed in rhizosphere soil than in bulk soil during all growth stages from vegetative to reproductive growth. Pyrosequencing assessment revealed that different community composition between rhizosphere and bulk soils at the phylum level; in particular, Proteobacteria were increased in rhizosphere soil during growth, while Acidobacteria and Firmicutes were decreased in rhizosphere. Analysis of operational taxonomic units revealed that the bacterial communities of the rhizosphere of soybean changed significantly during the growth in the field, with a higher abundance of bacterial with potential plant growth promoting properties, such as *Bacillus*, *Bradyrhizobium*, and *Rhizobium*, in a stage-specific manner. These findings demonstrated that soybean rhizosphere bacterial communities were changed during the growth in the field.

References

Sugiyama, Y. Ueda, T. Zushi, H. Takase, K. Yazaki, “Changes in the bacterial community of soybean rhizospheres during growth in the field,” *PLoS ONE*, vol. 9, no. 6, e100709, 2014

Sugiyama, Y. Ueda, T. Takase, K. Yazaki, “Do soybeans select specific species of *Bradyrhizobium* during growth?” *Communicative & Integrative Biology*, vol. 8, no. 1, e992734, 2015

RECENT RESEARCH ACTIVITIES

Application of an interferometric gravity gradiometer to measurement of soil moisture content

(Laboratory of Atmospheric Sensing and Diagnosis, RISH, Kyoto University)

Sachie Shiomi and Toshitaka Tsuda

Soil moisture content is an important factor for plant growth. Monitoring spatial and time variations of soil moisture content is essential for sustainable agriculture and forests. We are developing a novel method of measuring soil moisture content. In this method, gravity variations caused by soil moisture content are measured by an interferometer. Here, we briefly introduce the method and report the current status of the development.

Introduction

Widely used soil-moisture sensors are typically placed in the soil for measurement. As a result, the measured values are likely to contain errors associated with the physical properties and conditions of the soil, close to the sensors. Also, the representative values of soil moisture content in an area of interest are conventionally determined by measuring at one or several observation points. Because of the limited number of observation points, possible inhomogeneities in the soil are hardly detected. There is a good chance that the measured values are inappropriately used as the representative. In order to have a more precise profile of spatial and time variations of soil moisture content, we propose to use a gravity gradiometer.

The method

A gravity gradiometer is an instrument to measure gravity differences due to underground density variations. It is used by oil, gas and mining companies to explore underground resources. We intend to apply a new type of gravity gradiometer, developed for volcanological studies, to monitor soil moisture content. A detailed description of this gravity gradiometer is given in the reference: S. Shiomi, et al, *Journal of the Geodetic Society of Japan*, vol. 58, no. 4, pp. 131-139, 2012.

In this gravity gradiometer, a pair of test masses set at different heights is dropped in a vacuum tank. The free-fall motion of the test masses is monitored by an interferometer. Any difference in local gravitational fields, caused by changes in soil moisture content, affects the motion of the test masses. Therefore, by monitoring the free fall of the test masses with the interferometer, we can estimate the change in soil moisture content. It should be noted that the soil moisture content, estimated by this method, is the bulk average and not influenced by the physical conditions or properties of the soil. By forming an observation network of such gravity gradiometers in an area of interest and carrying out simultaneous measurements, we can have a real-time estimate of spatial and time variation of soil moisture content in the area.

Conventional gravimeters, such as spring and superconducting gravimeters, can also be used to monitor soil moisture content. However, these devices are susceptible to seismic vibration; it is difficult to carry out sensitive measurements in areas with high seismic vibration, such as volcanic and coastal areas. The interferometric gravity gradiometer, described above, was originally supposed to be used on an airship so that it is designed to be robust against vibrations.

The current status and future prospects

The first observation using the interferometric gravity gradiometer was carried out at a laboratory on Mt. Sakurajima in Kyusyu, one of the most active volcanos in Japan, in 2014. Its data analysis showed that the resolution was about one order of magnitude better than the one of previous gravity measurements, made at the same laboratory using a commercial absolute gravimeter. This result indicates that the gravity gradiometer has a high robustness. There is a good chance of having a high resolution even when used on a vehicle, such as a ship and airship, for fieldwork. We intend to carry out further development for onboard measurements in the future. Currently, we are tentatively taking measurements at a laboratory on the 1st floor of RISH to monitor the time variation of soil moisture content during the rainy season. We intend to understand the soil structure and the physical process of infiltration under the laboratory.

RECENT RESEARCH ACTIVITIES

Photochemical Aging Mechanism of Aqueous Organic Aerosols

(Laboratory of Atmospheric Environmental Information Analysis, RISH, Kyoto University)

Shinichi Enami

A major source of uncertainty in predicting the climate and health effects of organic aerosol is how its composition changes over their atmospheric lifetimes. Here, products and intermediates of the oxidation of atmospherically relevant aqueous di-carboxylic acids (DCAs) initiated by gas-phase hydroxyl radicals, OH(g), at the air-water interface were detected by mass spectrometry in a novel setup under various experimental conditions. Exposure of sub-millimolar reactant aqueous microjets to ~ 10 ns OH(g) pulses from the 266 nm laser flash photolysis of $O_3(g)/O_2(g)/H_2O(g)$ mixtures yielded an array of interfacial intermediates/products, including peroxyl radicals and peroxides, that were unambiguously and simultaneously identified in situ by mass spectrometry[1,2]. An important finding is that the oxidation of DCAs initiated by gas-phase OH radicals leads not only to their stepwise degradation but also to the formation of more reactive species, such as hydroperoxides, which can propagate radical chain reactions in the condensed aerosol phase. We demonstrate that the reactivities of shorter-chain DCAs homologues (oxalic acid and malonic acid) toward OH(g) decrease dramatically, in line with the higher hydrophilicity of the shorter chain mono-anions that inhibits their partitioning to the air-water interface. The present results would explain why and how shorter-chain DCAs naturally accumulate in aged organic aerosol. Our results suggest that interface-specific OH oxidation of DCAs would play a far more significant role in photochemical aging process of atmospheric aerosols than previously assumed.

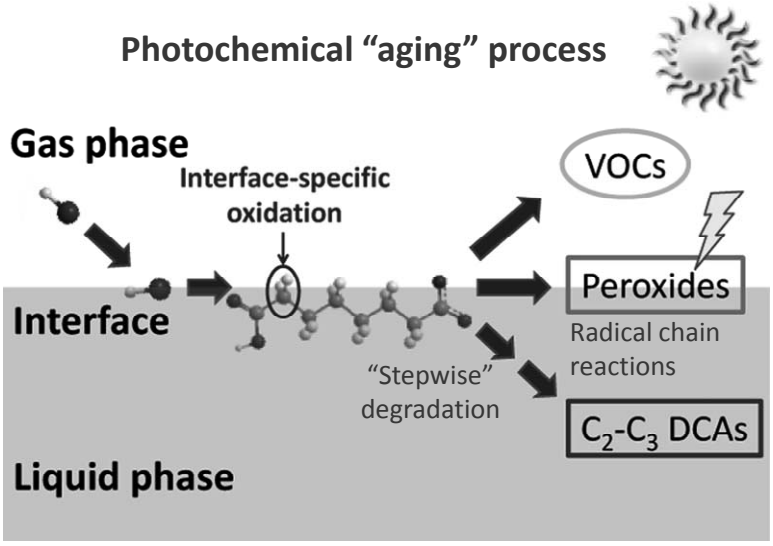

Figure 1. A mechanism of OH-initiated oxidation of dicarboxylic acid at the air-water interface

References

[1] Enami, S., *et al.*, “In situ mass spectrometric detection of interfacial intermediates in the oxidation of RCOOH(aq) by gas-phase OH-radicals” *J. Phys. Chem. A, 118*, 4130−4137, **2014**.

[2] Enami, S., *et al.*, “Stepwise oxidation of aqueous dicarboxylic acids by gas-phase OH-radicals” *J. Phys. Chem. Lett., 6*, 527–534, **2015**.

RECENT RESEARCH ACTIVITIES

Study on atmospheric turbulence based on simultaneous observations with the MU radar, lidar, and radiosondes

(Laboratory of Radar Atmospheric Science, RISH, Kyoto University)

Hiroyuki Hashiguchi, Hubert Luce, Richard Wilson, Masanori Yabuki, and Mamoru Yamamoto

Small-scale turbulence in the free atmosphere can be monitored from VHF radars as they are mainly sensitive to refractive index irregularities. The Middle and Upper atmosphere (MU) radar is one of the most powerful and flexible VHF radars of the world for studying atmospheric structure and dynamics. It was the first VHF radar to be operated in range imaging mode using frequency diversity. This observational mode makes possible to obtain detailed observations of turbulent events at unprecedented time and spatial resolutions (e.g., [1]). It can also make easier the identification of their sources such as dynamic shear instabilities and convective instabilities (e.g., [2, 3]). In parallel, improved processing methods for identifying turbulence from standard radiosonde data (sampled at 0.5 or 1 Hz) were proposed by Wilson et al. [4]. These methods, initially developed for oceanic data, are based on sorting vertical profiles of temperatures or densities conserved through adiabatic process. The vertical displacements are signatures of turbulent overturns. Because instrumental noise can generate artificial overturns in weakly stratified regions, we developed robust and objective methods for rejecting these spurious effects.

The purpose of our research is to get new insights on atmospheric turbulence (sources, energetic, scales, and so on) by combining the most performing radar, lidar, and balloon observation data and processing tools to date. We often carried out multi-instrumental campaigns at the Shigaraki MU Observatory including the MU radar, a UHF wind-profiler radar, lidars and radiosondes. Intensive radiosonde observations were carried out during night periods while the MU radar was continuously operated in range imaging mode. Various meteorological conditions were met during the different nights so that the characteristics of the turbulent events and their occurrence strongly differed. Figure 1 shows the example of the time-height cross section of echo power observed with the MU radar imaging mode. We found Kelvin-Helmholtz (KH) braided-like structures along the slope of a cloud base gradually rising with time at approximately 5.0 km altitude and vertical air motion oscillations exceeding ±3 m/s with a period of approximately 3 min above and below the cloud base.

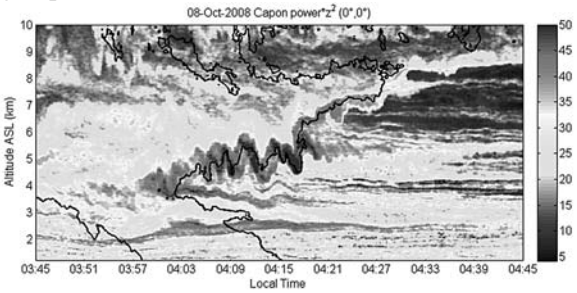

Figure 1. Time-height cross-section of echo power observed with the MU radar imaging mode on October 8, 2008. [5]

References

[1] Luce, H., G. Hassenpflug, M. Yamamoto, and S. Fukao, High-resolution vertical imaging of the troposphere and lower stratosphere using the new MU radar system, *Ann. Geophys.*, 24, 791–804, 2006.

[2] Luce H., N. Nakamura, M. K. Yamamoto, M. Yamamoto, and S. Fukao, MU radar and lidar observations of clear-air turbulence underneath cirrus, *Monthly Weather Review*, 138, 438-452, 2010.

[3] Fukao, S., H. Luce, T. Mega, and M. K. Yamamoto, Extensive studies of large-amplitude Kelvin-Helmholtz billows in the lower atmosphere with the VHF middle and upper atmosphere radar (MUR), *Q. J. R. Meteorol. Soc.*, 137, 1019–1041, doi:10.1002/qj.807, 2011.

[4] Wilson, R., F. Dalaudier, and H. Luce, Can one detect small-scale turbulence from standard meteorological radiosondes?, *Atmos. Meas. Tech.*, 4, 795–804, doi:10.5194/amt-4-795-2011, 2011.

[5] Luce, H., T. Mega, M.K. Yamamoto, M. Yamamoto, H. Hashiguchi, S. Fukao, N. Nishi, T. Tajiri, and M. Nakazato, Observations of Kelvin-Helmholtz instability at a cloud base with the middle and upper atmosphere (MU) and weather radars, *J. Geophys. Res.*, 115, doi:10.1029/2009JD013519, 2010.

RECENT RESEARCH ACTIVITIES

Nanofibrillation of dried pulp in NaOH solutions and their regenerations

(Laboratory of Active Bio-based Materials, RISH, Kyoto University)

Kentaro Abe, Hiroyuki Yano

Plant cell walls have a strong framework or scaffold consisting of nano-scale crystalline bundles of cellulose molecules, called microfibrils. Because of the stable structure provided mainly by inter/intramolecular hydrogen bonds, the crystal region displays strong mechanical properties longitudinally and low thermal expansion coefficient. In addition to these properties, because of their low weight and morphological features such as large specific surface areas and high aspect ratios, plant-based cellulose nanofibers have great potential for reinforcing polymer matrices.

A variety of fibrillation methods using mechanical treatment have been reported for the preparation of cellulose nanofibers, and currently nanofibers can be isolated from various plant sources. We have also reported an isolation method in which plant fibers are ground in an undried state, and have prepared cellulose nanofibers from various sources such as softwood, rice straw, potato tuber and bamboo[1-3].

However, when dried pups are used as a raw material, the drying process production generates strong hydrogen bonding between cellulose microfibrils after the removal of the matrix, which seems to make it difficult to obtain thin and uniform cellulose nanofibers. On the other hand, it is well known that alkali solutions swell cellulose fibers. It means that alkali-swelling may loose the hydrogen bond between microfibrils and facilitate the nanofibrillation. In the present study, we tried the fibrillation of pulps under alkaline condition in order to obtain fine nanofibers from dried pulps. The fibrillation of dried pulps was executed in 8% or 16% of NaOH using a bead-milling method.

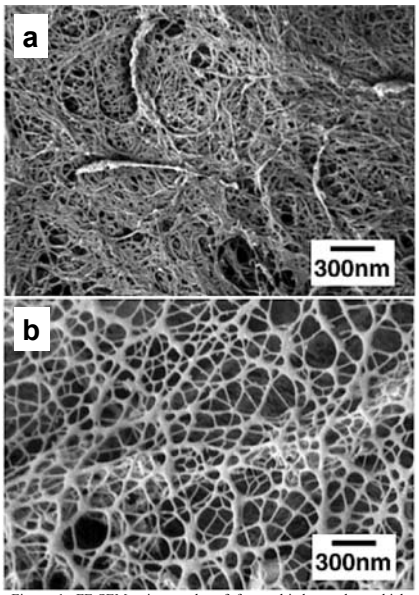

Figure 1. FE-SEM micrographs of freeze-dried samples, which were fibrillated using a beads-milling in 8 wt% (a) and NaOH (a–c) and 16 wt% NaOH (b) and then neutralized.

As a result, the bead milling method in 8 wt% NaOH succeed to fibrillate the dried pulp into uniform nanofibers with a width of approximately 12 nm (Fig. 1a), which corresponds to the cellulose microfibril aggregates in wood cell wall. On the other hand, when fibrillated in 16 wt% NaOH, the sample neutralized showed a continuous and uniform network with a width of 12-30 nm (Fig. 1b). Moreover, it was found that both of nanofiber suspensions treated in 8 wt% or 16 wt% NaOH were formed into a stable hydrogel by neutralization. Such gelation behavior is most likely caused by the interdigitation of the neighboring nanofibers during NaOH treatment (mercerization)[4, 5]. This method can be applied to prepare wet-spun fibers based on cellulose nanofiber.

References

[1] Abe K, Iwamoto S, Yano H. *Biomacromolecules*. **8**: 3276-3278, 2007.

[2] Abe K, Yano H. *Cellulose* **16**: 1017-1023, 2009.

[3] Abe K, Yano H. *Cellulose*. **17**: 271-277, 2010.

[4] Abe K, Yano H. *Carbohydrate Polymers*. **85**: 733–737, 2011.

[5] Abe K, Yano H. *Cellulose*. **19**: 1907–1912, 2012.

RECENT RESEARCH ACTIVITIES

Development of particleboard made from bagasse of sweet sorghum (*Sorghum bicolor* L. Monech) and citric acid

(Laboratory of Sustainable Materials, RISH, Kyoto University)

Sukma Surya Kusumah, Kenji Umemura, Kozo Kanayama

Development of wood-based composite made from wood material and citric acid has been researched in recent years [1-3]. However, wood resources have been continuously decreased year by year due to decreasing of forest land. Therefore, agricultural wastes such as sugarcane bagasse, rice straw, and sorghum bagasse become important resources as alternative raw materials of wood-based composite [4]. In Indonesia, new kind of sweet sorghum called "super hybrid sweet sorghum" has been especially planted in large field as multipurpose plant. Hence, the large quantities of sorghum bagasse will be generated and cause the greenhouse gas emission. As one of the effort to resolve the problem, there is a utilization of sorghum bagasse as raw material for wood-based composite such as particleboard. In this study, the manufacture of particleboard using super hybrid sweet sorghum bagasse (SHSSB) and citric acid was attempted. The effects of citric acid content on the physical properties were investigated.

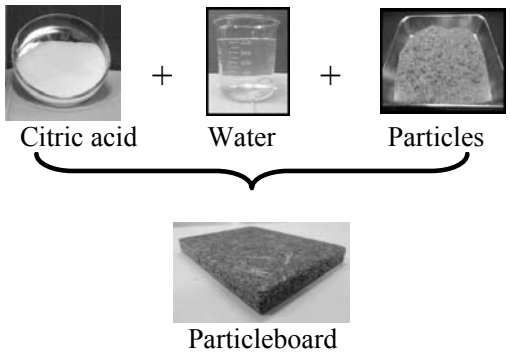

Figure 1. The production of particleboard from super sweet sorghum bagasse and citric acid.

Materials

The SHSSB particles as raw materials were obtained from Innovation Center, Indonesian Institute of Sciences (LIPI). The particles remaining between aperture size of 5.9 and 0.9 mm of sieving machine were dried in an oven at 80 ^{o}C for 12 h. Citric acid was dissolved in water until the solution concentration of 59 wt%.

Production and evaluation of particleboard

Particleboards bonded with citric acid in the several of resin contents i.e. 0~30 wt% were manufactured under a press condition of 200 ^{o}C for 10 min. The particleboard size and target density were 300 x 300 x 9 mm and 0.8 g/cm^3, respectively. The board were conditioned at 20 ^{o}C and 60% of relative humidity for 1 week. The bending properties, internal bonding (IB) strength, and thickness swelling (TS) of the board were investigated according to JIS A 5908 (2003) standard [5].

Effect of citric acid contents

The bending properties, IB strength, and TS of the particleboard were improved with increasing citric acid content. The board bonded with 20 wt% citric acid had maximum average values of modulus of rupture (MOR) and modulus of elasticity (MOE) i.e. 19.60 MPa and 4.67 GPa, respectively. Meanwhile, IB of the board bonded with 20 wt% citric acid was lower than 30 wt% citric acid. The board bonded with 30 wt% citric acid had lowest TS (13.45%). Mechanical properties of particleboards bonded with 20 and 30 wt% citric acid were comparable to the standard of JIS A 5908 (2003) 18 type, whereas TS of particleboards didn't satisfied with JIS standard. Further study will be performed to clarify the effect of manufacturing conditions on the physical properties of the particleboard.

References

[1] Umemura K, T Ueda, SS Munawar, S Kawai. 2012. J. Appl. Poly. Sci. 123: 1991 – 1996.
[2] Umemura K, T Ueda, S Kawai. 2012. J. Wood. Sci. 58: 38 – 45.
[3] Umemura K, O Sugihara, & S Kawai. 2013. J. Wood Sci. 59: 203-208.
[4] Zini E and M Scandola. 2011. Polymer Composite. 32 (12): 1906 – 1915.
[5] [JIS] Japanese Industrial Standard. 2003. Japanese Standard Association. Tokyo. Japan.

RECENT RESEARCH ACTIVITIES

Development of CLT panels bond-in method for seismic retrofitting of RC frame structure

(Laboratory of Structural Function, RISH, Kyoto University)

Ryota Haba, Akihisa Kitamori, Takuro Mori and Hiroshi Isoda

1. INTRODUCTION

CLT is a multi-layer wooden panel made of lumber. Each layer of boards is placed crosswise (typically at 90 degrees) to the adjacent layers for increased rigidity and stability. The panel can have three to seven layers or more, normally in odd numbers, symmetrical around the mid layer. Dimensional lumber is the main input material. It can be composed at the factory once the panel is assembled. The effective use of wood for CLT is expected to contribute to sustainable development of forestry. However, there are not so many ways to use CLT in Japan.

2. OBJECTIVE

Many RC buildings built before 1981 need seismic retrofit at present in Japan. Installing new RC shear walls or steel braces in RC frame is one of the seismic retrofit techniques at present. We are suggesting new seismic retrofit method using CLT panels as shear walls. In this method, setting small CLT panels in RC frame and bonding each panel and panel to RC frame with epoxy resin, panels compose shear walls. The advantages of this technique are: There are less dust, noise, and vibration during construction; Light weight panels enable easy construction and short construction period; Light weight panel also lead small seismic force.

3. EXPEIRMENTAL METHODS

CLT panels which are used in this test consist of different grade Japanese cedar. These are 3 layer/3-ply, the size of 214mm x1540mm, and 30mm thick. Seven or four pairs of CLT panels are set in a line in the RC frame. And they are bonded each other and to the RC frame with epoxy resin on-site. Fig.1 shows four types of specimens in this test. These are intended to apply to several kinds of actual seismic retrofitting.

4. TEST RESULT & DISCUSSION

So far we have found that every reinforced specimen is stiffer, stronger, and more ductile than the plain RC frame. This result satisfies actual seismic retrofitting properties. By analyzing this mechanical resisting model, we are studying to propose design manual for this retrofitting technique.

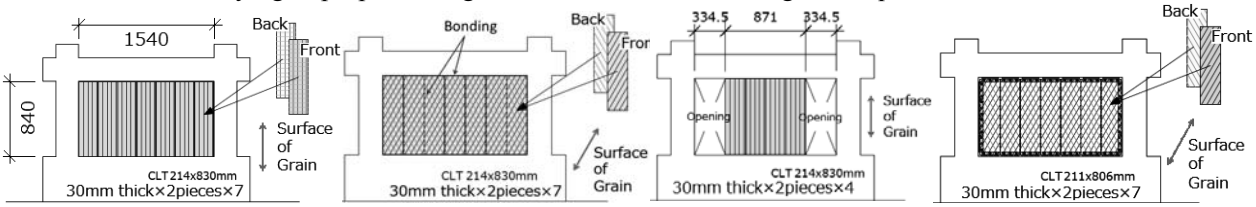

T type X type T-O type X-S type

Fig1: Specimens

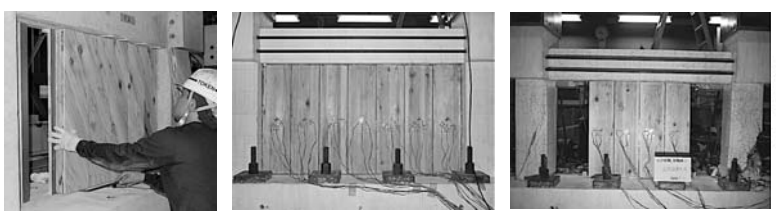

Fig 2: Setting panels(left), Test(middle), Damage(right)

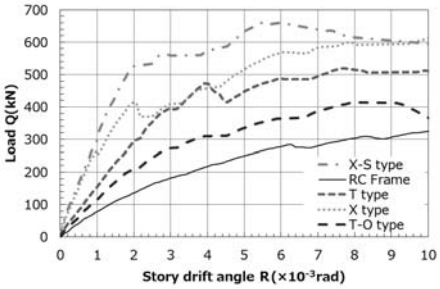

Fig3: Load-Displacement

RECENT RESEARCH ACTIVITIES

International collaboration work with a group in France

(Laboratory of Innovative Humano-habitability, RISH, Kyoto University)

Aya Yanagawa

Recently I have been working with the Marion-Poll lab in Center national de la recherche scientifique (CNRS), the largest governmental research organization in France, to analyze how Drosophila can detect microbes with their taste system and brush them of their cuticula to limit pathogenic infections. This collaboration work has started in 2013 with the generous support of Kyoto University on John Mung Program and we keep continuing this collaboration project in Japan and France. Though the collaboration level is not large, we could produce the first paper in 2014, last year and I'd like to share that work here.

Bacterial compounds induce grooming and stimulate taste sensilla on the wings of Drosophila

In many insects, grooming is considered as a behavioural defence against pathogen and parasite infection since it contributes to remove microbes from their cuticle. However, the stimuli that trigger this behaviour are not well characterized. In this work, we demonstrate that grooming activities in *Drosophila melanogaster* are induced by taste stimuli. We monitored the grooming responses of decapitated flies to general tastants (quinine, sucrose, KCl), to bacterial compounds e.g. dead *Escherichia coli* (Ec) and lipopolysaccharides (LPS). Grooming responses were triggered most efficiently when touching the distal border of the wings, in response to quinine, LPS and Ec while the responses were completely absent in mutants deprived of external taste sensilla. We monitored the electrophysiological responses of taste sensilla of the distal border of the wings, confirming that these taste sensilla are fully functional, and that they respond not only to quinine, Ec and LPS but also to sucrose and KCl. These results demonstrate for the first time that wing taste sensilla detect chemicals from bacteria, and that these sensilla are directly involved in triggering grooming movements driven by the ventral nerve cord. This work is published in Frontiers in behavioral neuroscience (2014: doi: 10.3389/fnbeh.2014.00254).

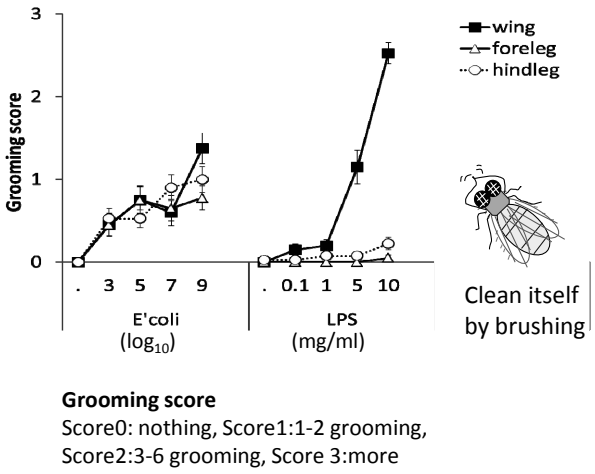

Fig.1 Grooming induction by bacterial compounds

Acknowledgements

I am deeply appreciated that Prof. F. Marion-Poll (CNRS, France) for his thoughtful supervisions and support throughout the project. The author is grateful to Dr. A. Guigue (Swedish University of Agricultural Sciences, Sweden), Dr. A. French (Imperial College London, UK), whole team members in his laboratory and the compartment of Laboratoire Evolution, Genomes, Comportement et Ecologie (CNRS, France). I thank Dr K. Scott (University of California, US), Prof. J. Carlson (Yale University, US), Dr L. Soustelle (University of Montpellier I and II, France) and Dr Y. Grau (University of Montpellier I and II, France) for the fly strains, Dr. E. Jacquin-Joly (INRa, France) for the *E. coli* strain used in this study and Dr. T. Yanagawa (Kurume University, Japan) for guidance and comments about statistical analysis.

RECENT RESEARCH ACTIVITIES

Simulations and Modeling of Geospace Environment

(Laboratory of Computer Space Science, RISH, Kyoto University)

Yoshiharu Omura and Yusuke Ebihara

We gave a brief account of the nonlinear theory of the generation mechanism of chorus emissions, which has been revealed by the simulations and observations. We described the nonlinear dynamics of resonant electrons, and the formation of the electromagnetic electron "hole" that results in resonant currents generating rising-tone emissions. In contrast, falling-tone emissions are generated through the formation of electron "hills." We also described the mechanism of nonlinear wave damping due to quasi-oblique propagation, which results in the formation of a gap at half the electron cyclotron frequency. The nonlinear wave-growth theory of chorus emissions can also be applied to the generation mechanism of electromagnetic ion-cyclotron (EMIC) triggered emissions, recently found in spacecraft observations. Hybrid code simulations confirmed that coherent rising-tone emissions are generated by energetic protons at frequencies below the proton cyclotron frequency. Electromagnetic ion-cyclotron waves can also interact with relativistic electrons. Both chorus emissions and electromagnetic ion-cyclotron-triggered emissions play important roles in controlling radiation-belt particle dynamics [Omura, Radio Sci. Bull., 2014].

We performed parametric analyses of electromagnetic ion cyclotron (EMIC) triggered emissions with a gradient of the nonuniform ambient magnetic field using a hybrid simulation. According to nonlinear wave growth theory, as the gradient of the ambient magnetic field becomes larger, the theoretical threshold of the wave amplitude becomes larger, although the optimum wave amplitude for nonlinear wave growth does not change. With a larger magnetic field gradient, we obtain coherent rising-tone spectra because the triggering process of the EMIC triggered emission takes place only under a limited condition on the wave amplitude. On the other hand, with a smaller magnetic field gradient, triggering of the emissions can be caused with various wave amplitudes, and then the subpackets are generated at various locations at the same time. The concurrent triggering of emissions results in incoherent waves, observed as "broadband" EMIC bursts [Shoji and Omura, J. Geophys. Res., 2014].

We surveyed the THEMIS probe data and found various types of emissions mainly on the dayside at radial distances of 6–10 RE. We studied three distinctive events in detail. The first is a typical event with an obvious rising tone emission in the afternoon sector. The emissions in the second event are simultaneously excited in different frequency bands separated by the cyclotron frequency of helium ions. In the third event, which occurred near local noon, rising tone emissions were excited in an extended region near the equator where the field-aligned B gradient was much reduced because of compression of the magnetosphere by the solar wind. We compared these events with the nonlinear wave growth theory developed by Omura et al. (2010). In all events, the observed relationship between the amplitudes and frequencies of the emissions are in good agreement with the theory [Nakamura, Omura et al., J. Geophys. Res., 2014].

A substorm is known to be one of the most drastic phenomena in the near-Earth space environment. The substorm redistributes the particles trapped by Earth's magnetic field. Utilizing a global magnetohydrodynamics (MHD) simulation, we demonstrated for the first time that the direction of the convection electric field is reversed just after a substorm. Calculated magnetic disturbances on the ground from pole to equator are consistent with those observed [Ebihara, Tanaka and Kikuchi, J. Geophys. Res., 2014]. We identified that the high-pressure region retreats tailward in the plasma sheet just after the substorm onset. The variations of the pressure, the magnetic field, and the velocity are consistent with the MHD simulation [Yao, Ebihara and Tanaka, J. Geophys. Res., 2015]. Utilizing a test particle simulation, we investigated an entry process of the oxygen ions originating from the ionosphere to the inner magnetosphere. The ions are accelerated non-adiabatically from ~eV to ~10^5 eV in the plasma sheet just after the onset. A "void" structure appears in the energy-time spectrogram of the phase space density of the ions, which results from quasi-electrostatic acceleration taking place in the stretched plasma sheet [Nakayama, Ebihara and Tanaka, J. Geophys. Res., 2015].

RECENT RESEARCH ACTIVITIES

Standardization and Scientific Society Activities for Wireless Power Transfer, Solar Power Satellite/Station, and Microwave Processing

(Laboratory of Applied Radio Engineering for Humanosphere, RISH, Kyoto University)

Naoki Shinohara, Tomohiko Mitani, Yohei Ishikawa, Junji Miyakoshi, and Shin Koyama

We introduce established industrial consortiums and scientific society to promote our technologies of a wireless power transfer (WPT), Solar Power Satellite/Station (SP), and microwave processing.

WiPoT (Wireless Power Transfer Consortium for Practical Applications)[1] was established by Prof. Shinohara as the first chair with 22 companies and 24 university's members on April, 2013.In the end of FY2014, number of companies member is 29 and number of university's member is 38. We mainly discuss to promote a WPT via microwaves. On August, 2014, we invited an engineer of PowerCAST company, which produce an receiver of a wireless power in US, and discuss a future collaboration. The WiPoT collaborates with European WPT consortium named WIPE (Wireless Power Transmission for Sustainable Electronics).

WPMc (Wireless Power Management Consortium) was also established by Prof. Shinohara as a chair and Dr. Hosotani of Murata Corporation as the first vice chair in 2013. The WPMc promotes a direct current resonance coupling WPT technology with 36 company members.

KID-S(Kaiyo Inverse Dam Society) was established by Prof. Ishikawa as a chair in 2013 to promote an inverse dam on marine for renewable energy and SPS with 11 companies. The KID-S is a general incorporated association.

Laboratory members work hard for international and domestic scientific society. In Microwave Theory and Technique Society of IEEE (The Institute of Electrical and Electronics Engineers, Inc., USA), new international conference of wireless power transfer (WPTc) was established. In 2014, the 2nd WPTc was held in Jeju Island, Korea, and Prof. Shinohara works for the WPTc as a founder of the conference and member of advisory committee. Number of attendees was approximately 200. Prof. Shinohara works for international journal of the WPT in Cambridge Press, England as one of executive editors[4].

Dr. Mitani and Prof. Shinohara works as board members on Japan Society of Electromagnetic Wave Energy Applications (JEMEA)[5] to promote microwave processing and microwave chemical science. They also belong to No. 188 committee (Reactive Field Excited by Electromagnetic Waves)[6] at JSPS (Japan Society for the Promotion of Science) which was established in 2014.

The Space Solar Power Systems (SSPS) Society was established in 2014[7] and Prof. Shinohara is one of its board members. The SSPS Society aims to promote the SPS in Japan.

Prof. Miyakoshi is a membership committee chair of Bioelectromagnetics Society (BEMS) (USA), a working group member of World Health Organization (WHO) - International Agency for Research on Cancer (IARC), WHO-EMF Project-Task Group Member, and SCII Member of International Commission on Non-Ionizing Radiation Protection (ICNIRP). He also works for 'new regional research' with Dr. Koyama in RISH.

Our hope is a sustainable humanosphere with such new technologies with international collaborations.

References

[1] WiPoT http://www.wipot.jp/english/
[2] WPMc http://wpm-c.com/ (in Japanese)
[3] KID-S http://kid-s.jpn.com/enterprise/ (in Japanese)
[4] Journal of WPT http://journals.cambridge.org/action/displayJournal?jid=wpt
[5] JEMEA http://www.jemea.org/?ml_lang=en
[6] No.188 committee of JSPS https://www.jsps.go.jp/j-soc/list/188.html (in Japanese)
[7] SSPS society http://www.sspss.jp/ (in Japanese)

RECENT RESEARCH ACTIVITIES

Novel Space Environment Monitor, Instrument, and Space Mission Concepts

(Laboratory of Space Systems and Astronautics, RISH, Kyoto University)

Hiroshi Yamakawa, Hirotsugu Kojima, and Yoshikatsu Ueda

Space Debris Observation, Trajrctory, and Mitigation

The space debris problem is tackled from observation (space situational awareness), trajectory evolution, and mitigation points of view. 1) A method to identify known space debris using MU (Middle and Upper) Radar of RISH, Kyoto Universiry, is investigated with some successful observation results. 2) An on-orbit space debris observing system is studied assuming an optical sensor onboard a satellite. 3) Space debris trajectory evolution is investigated focusing on objects smaller 10 cm. 4) Space debris mitigation (orbit control) using Lorentz force by positive charging effect is studied. The interaction between an electro-statically charged debris and the Earth's plasma environment is investigated. The orbit control method to decrease the altitude using Lorentz force is also studied.

Magneto-Plasma Sail and Electric Sail Space Propulsion System

A Magneto-Plasma Sail (MPS) is a unique propulsion system, which travels through interplanetary space by capturing the energy of the solar wind, which inflates a weak original magnetic field made by a High-Temperature Super-conducting (HTS) coil of several m in diameter with an assistance of a high-density plasma jet. We investigated the methods to maximize the thrust capability by increasing the thrust to mass ratio. The approaches we took are 1) optimizing the HTS coil design to increase the current and maximize its magnetic moment within the capacity of the space vehicle, and 2) developing a deployable HTS coil with a larger diameter to increase the coil area and magnetic moment in space. An Electric Sail (ES) is a space propulsion system by positively charging the extended wires attached to the spacecraft body, which captures the momentum of the solar wind. The thrust of the ES is evaluated and applied for deflecting near-Earth asteroids which has a possibility of approaching the Earth in the near future.

Miniaturization of plasma wave receiver system

To meet the recent requirements on the size, mass and power budgets in constellation missions or planetary missions, the miniaturization of plasma wave receiver is inevitable. The attempt to realize the extremely miniaturized plasma wave receiver have been made using analogue ASIC technology in the lab. The main activity in 2012 is the success in the development of the tiny waveform capture receiver, which is one of the typical types of plasma wave receivers. The size of the developed tiny waveform receiver is about one tenth of the conventional waveform receiver. Moreover, we also succeeded in implementing the preamplifier and the calibration system on the same analogue chip of the waveform receiver.

Quantitative evaluation of electrochemical properties of fine-bubbles in water based on the type of gas

Recently, fine bubble (FB) has found applications in various fields. We have reported the effectiveness of water containing FB water of approximately 100 nm diameter for removal of radioactive cesium from soil and gravel conglomerate and nonwoven cotton. In Fukushima, this method of radioactive contamination removal using FB water is currently under trial. We also investigated the freshness-keeping effect of water containing FB on cut flowers such as a gentian, a lisianthus, and a small chrysanthemum. Although there were statistical dispersions in experimental results, FB was effective in keeping the freshness in the experiments. We focused our attention on the electrochemical properties of pure water (such as pH and electrical conductance) containing FB; we evaluated their correlation with the concentration of FB and investigated their potential for use as parameters for the characterization of FB in water.

ABSTRACTS (PH D THESIS)

Development of a Rectenna Adapted to Ultra-wide Load Range for Microwave Power Transmission

(Graduate School of Engineering, Laboratory of Laboratory of Applied Radio Engineering for Humanosphere, RISH, Kyoto University)

Yong Huang

Numerous studies have been carried out on the wireless power transmission (WPT) technologies, which transfers power to the electrical loads without man-made wires. As one mean of WPT, microwave power transmission (MPT) has attracted lots of attention due to its long-distance power transmission capability. Figure 1 shows a block diagram of a MPT system. A notable problem among these technologies is that the RF to DC conversion efficiency could be easily affected by the load resistance and the input power. Therefore, an impedance matching circuit becomes crucial to realize the wireless power transmission with high efficiency. Moreover, most of the impedance matching circuits in microwave circuits utilize distributed-constant circuits, whereas, the rectenna is a special distributed-constant circuit yielding a DC output. This present thesis aims at developing an ultra-wide load range rectenna for microwave power transmission and a resistance matching circuit from the viewpoint of DC, which is easy to design since it is unnecessary to consider high harmonics.

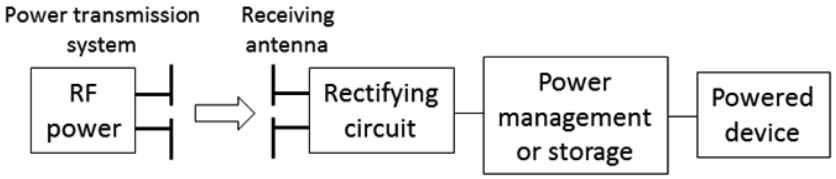

Figure 1. Block diagram of a MPT system.

Different from the conventional DC-DC converters used for voltage conversion, in the present thesis, a resistance conversion DC-DC converter is proposed and validated in the following procedures:

Firstly, with aid of the simulator of advanced design system (ADS), a common pulse-width modulation (PWM) controlled boost converter is checked as an impedance matching circuit for rectifying circuit. For the validation a simulation model of RF-DC-DC circuit is built which consists of a simple single shunt rectifying circuit and the boost converter. The simulation results show that the overall efficiency of the RF-DC-DC circuit is almost constant over 70% in the load range from 370 to 1300 Ω. Moreover, it is also found that the boost converter can prevent the reverse voltage applied on the rectifying diode from exceeding breakdown voltage and then the rectifying circuit can keep acting at the peak efficiency point. However, this PWM controlled boost converter can only convert a wide load range into a narrow input resistance range which is insufficient for an impedance matching requirement of rectenna.

Next, according to the previous simulation results, an RF-DC-DC circuit is shown to be useful for impedance matching application. Therefore, an externally powered RF-DC-DC circuit, consisting of a negative output rectifying circuit and a DC-DC converter, is designed. To choose a more suitable type of DC-DC converter, the input/output resistance relationships of three major DC-DC converter topologies (i.e. buck converter, boost converter and buck-boost converter) are investigated in continuous conduction mode (CCM) and discontinuous conduction mode (DCM), respectively. Only the DCM buck-boost converter is found to exhibit constant input resistance characteristic independent of the input voltage and the load resistance. Therefore, an inverting DCM buck-boost converter is adopted with an extra DC power supply for the control-pulse circuit, and the input resistance of the buck-boost converter is set to be close to the optimal load of the rectifying circuit. The experimental results show that the overall efficiency of this externally-powered RF-DC-DC circuit is approximately constant and over 60 %, despite the load resistance ranging from 100 to 5000 Ω.

ABSTRACTS (PH D THESIS)

However, the externally-powered RF-DC-DC circuit is difficult for the practical applications because of the requirement of an extra DC power supply. To solve this problem a self-powered RF-DC-DC circuit consisting of a positive output rectifying circuit and a non-inverting self-powered buck-boost converter (as shown in Fig. 2) is proposed. It can obtain a positive output voltage with a single positive input voltage. Furthermore, the input resistance of the buck-boost converter is designed to be equal to the optimal load of the rectifying circuit. The experimental results are shown in Fig. 3. We can see that the overall efficiency of the self-powered RF-DC-DC circuit is constant and over 66 %, despite an ultra-wide load ranging from 200 to 10000 Ω.

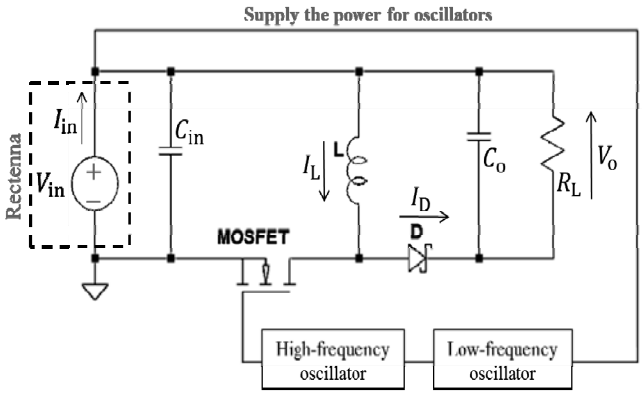

Figure 2. Block diagram of a non-inverting self-powered buck-boost converter.

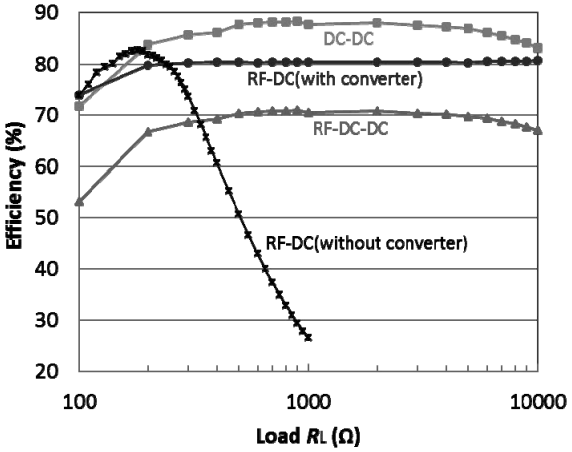

Figure 3. Experimental efficiency comparison of the RF-DC-DC circuit and the general rectifier.

Finally, several experiments are carried out on driving a DC motor using MPT with a compact designed power-receiving device which consists of a rectenna array (including antennas and rectifiers) and an improved buck-boost converter. There exits four types of power-receiving devices combined by two different rectenna arrays and two different buck-boost converters. With these four power-receiving devices, some experiments are conducted by driving a dynamic load resistance device such as a DC motor with continuous-wave (CW) power transmission and pulsed-wave power transmission. Figure 4 shows the block diagram of experiment setup for driving DC motor with pulsed-wave. In the CW case, the overall efficiency of the compact power-receiving device is above 50% in a wide power density ranging from 0.25 to 2.08 mW/cm^2. In the pulsed-wave case, the overall efficiency is above 44% in the duty ratio ranging from 0.2 to 1 for a power density of 0.98 mW/cm^2. Moreover, at a fixed duty ratio of 0.5, the overall efficiency is almost constant at 59% with the pulsed-wave frequency changing from 0.33 to 41.7 kHz.

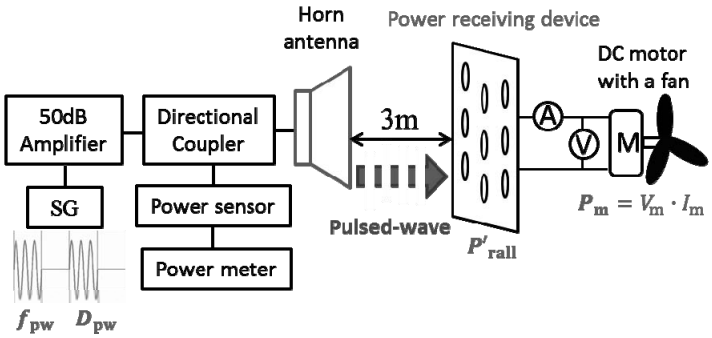

Figure 4. Experiment setup for driving DC motor by MPT using pulsed-wave.

Therefore, tested by both load resistances and a dynamic load resistance device, the proposed rectenna is found to be excellent in a relatively high efficiency for an ultra-wide load range. As a novel application of DC-DC converter, the proposed buck-boost converter, with constant input resistance characteristic, is also expected to be valuable for other WPT applications.

ABSTRACTS (MASTER THESIS)

A preliminary study for purifying the full complex cellulose synthase

**(Graduate School of Agriculture,
Laboratory of Biomass Morphogenesis and Information, RISH, Kyoto University)**

Kaho Mitani

Cellulose is an abundant biopolymer on Earth, and it is synthesized at cell membrane by cellulose synthase complex (CSC), a complicated protein complex composed of several different subunits. In a famous cellulose-producing bacterium, *Gluconacetobacter xylinus*, it is thought that CSC is an assembly of at least four different polypeptide subunits: CesA, CesB, CesC, and CesD. Recently X-ray crystallographic analysis [1] revealed a three-dimensional structure of CesA/CesB complex, which allowed for a big progress of understanding the polymerization mechanism of cellulose in cellulose synthase. Yet it will be necessary to reveal the three dimensional structure of full complex for understanding another important mechanism of cellulose synthase, crystallization/spinning mechanism to produce cellulose into an apparent single crystal of cellulose microfibril.

To this end, we tried to purify cellulose synthase full complex by using *E. coli* expression system.

Experiments and Results

CesA, CesB, CesC, and CesD proteins from *G. xylinus* were co-expressed in *E. coli* by using a conventional expression vector. A detailed procedure how to prepare the expression vector will be described elsewhere. Hexa-histidine tag was fused at the C-terminus of CesD protein (CesD-His6).

Total membrane (mixture of inner and outer membrane of a gram-negative bacterium like *E. coli*) was isolated from *E. coli* cells expressing the four proteins by a conventional protocol of differential centrifugation. Solubilized fraction of membrane proteins with detergent was processed with immobilized metal affinity chromatography (IMAC) with a nickel agarose to trap CesD protein and any other proteins, if any, which interact with CesD protein. Eluted fraction from IMAC was analyzed by western analysis with SDS-PAGE.

Western analysis showed that CesA protein was found together with CesD-His6 protein in the IMAC elute while CesB and CesC were not found. This indicates a direct interaction between CesA and CesD protein. Given that CesA is known to form a complex with CesB protein [1], CesA, CesB, and CesD are included in the bacterial CSC. The other subunit CesC, which is supposed to be anchored in outer membrane, was not even solubilized by detergent as far as we have tried. Compiling our result and the previous knowledge together, we putatively hypothesize that CesA protein has an interaction with each of CesB and CesD (Figure 1): CesD is supposed to interact with CesA outside the cell given the interaction with cellulose [2].

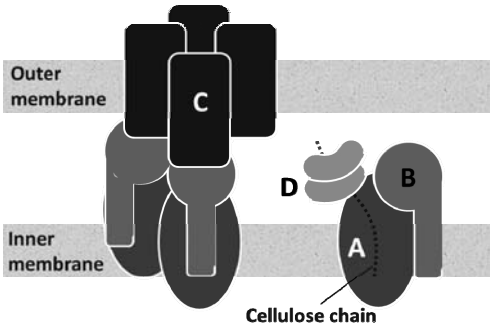

Figure 1. A putative model for the CSC of *Gluconacetobacter*: A, B, C, and D stand for CesA, CesB, CesC, and CesD subunits, respectively.

Acknowledgements

A part of the data was obtained by LC-IT-TOF analysis at DASH/FBAS in CER/RISH, Kyoto University.

References

[1] Morgan, J. L. W., Strumillo, J., and Zimmer, J., "Crystallographic snapshot of cellulose synthesis and membrane translocation", *Nature*, 493, 181-186, 2013.

[2] Hua, S.-Q., Gao,Y.-G., Tajima, K., Sunagawa, N., Zhoua, Y., et al. "Structure of bacterial cellulose synthase subunit D octamer with four inner passageways", *PNAS*, 110, 17957-17961, 2010.

ABSTRACTS (MASTER THESIS)

Degradation of lignocellulosic biomass by activated manganese porphyrin complexes

(Graduate School of Agriculture, Laboratory of Biomass Conversion, RISH, Kyoto University)

Ryo Iguchi

Lignin, a heterogeneous phenylpropanoid structural polymer of vascular plants, is the most abundant renewable material next to cellulose, but it hinders separation of cell wall polymers, cellulose and hemicelluloses. Therefore, extensive studies have been made to degrade lignin by chemical, enzymatic and microbial treatments of woody materials. Metalloporphyrins have been used as peroxidase models, and applied to lignin degradation. However, behavior of the biomimetic catalysts against natural woody biomass is not well understood. In this study, manganese porphyrin complexes with two different counter ions, Cl^- and AcO^- were synthesized and applied to degradation of a non-phenolic lignin dimer model compound and Japanese cedar wood. The Mn complexes with Cl^- did not efficiently decompose the model compound, but substitution of the counter ion to AcO^- significantly accelerated the degradation. This phenomenon can be explained by electron-donating properties of AcO^- which induced heterolysis of the peroxo complex of the manganese porphyrin complexes. Due to the high reactivity of the catalyst, softwood was degraded by the catalyst, and degradation of wood cell wall components were analyzed by 2D-NMR. The NMR spectra indicated that hemicelluloses and lignin were preferentially degraded at elevated temperatures.

ABSTRACTS (MASTER THESIS)

Ion-reducing polypeptides from white rot fungus

(Graduate School of Agriculture, Laboratory of Biomass Conversion, RISH, Kyoto University)

Yoshitaka Tokunaga

Continued usage of fossil fuels has caused depleted energy problems and serious environmental issues such as global warming. Therefore, production of energy and chemicals from the most abundant renewable resources, woody biomass is an urgent task for ensuring sustainability of our life. In biological conversion of woody biomass, selective lignin degradation is a key process because cell wall polysaccharides in wood are surrounded by lignin. In nature, the degradation of lignin in wood occurs primarily through the action of lignin-degrading basidiomycetes called white rot fungi; consequently, this ecological group has received a considerable amount of research attention. Most of white rot fungi simultaneously decompose lignin and cellulose, accompanied by erosion of wood cell walls, while some fungi called selective white rot fungi, such as *Ceriporiopsis subvermispora* are able to degrade lignin without intensive damage of cellulose. Thus, a white rot fungus *C. subvermispora* is useful for the production of bioethanol, biomethane, pulp and feed for ruminant animals due to its selective lignin-degrading ability. This fungus secretes hydrophobic metabolites such as fatty acids and alk(en)ylitaconic acids (ceripiric acids). These metabolites play important roles in the selective lignin-degrading system. In this study, extracellular polypeptides secreted by the fungus were analyzed by using the assay for Fe (III) and Cu (II) reduction. After purification by ammonium sulfate precipitation and gel permeation chromatography, the polypeptide fraction was separated. 2D-Elecrtophoresis demonstrated that at least two polypeptides were involved in the fraction. The peptides may play a role in extracellular redox reactions of this fungus to promote the lignin degradation by free radial process.

ABSTRACTS (MASTER THESIS)

Bioethanol production from fast-growing wood by simultaneous saccharification and co-fermentation

(Graduate School of Agriculture, Laboratory of Biomass Conversion, RISH, Kyoto University)

Ryo Toshima

In bioethanol production, pretreatments separating plant cell wall components produces fermentation inhibitors such as furfural, 5-hydroxymethylfurfural (5-HMF), vanillin, vanillic acid, syringaldehyde, syringic acid, acetic acid and other organic compounds from the cell wall polysaccharides and lignin. Molecular breeding of inhibitor-resistant ethanologenic microorganisms and process engineering to remove fermentation inhibitors have been studied for the production of bioethanol. Higher substrate concentration is needed to produce bioethanol at a lower cost. However, this demand, like the harsh pretreatment conditions, requires a concomitantly high level of technology to suppress the fermentation inhibition. So far, a number of technologies have been employed for removing inhibitors. However, the cost of bioethanol production is increased by additional processes, and the use of purchased adsorbent for fermentation inhibition is impractical for the production of biofuels, with a low cost that is competitive in the market. To overcome problems caused by fermentation inhibitors, bioethanol production process using residual lignin as an adsorbent for fermentation inhibitors was analyzed. *Eucalyptus globulus* wood was pretreated by microwave-assisted hydrothermolysis and separated into soluble and insoluble fractions by engineered *Zymomonas mobilis*. The two fractions were subjected to simultaneous saccharification and co-fermentation (SSCF) in combination with enzymatic pre-hydrolysis. After fermentation, the residual lignin was separated, and thermally processed to increase the adsorptivity for the inhibitory compounds. Effects of the adsorbent on reduction of inhibitors and bioethanol production by SSCF were analyzed.

ABSTRACTS (MASTER THESIS)

RNA-Seq analysis of shikonin-producing *Lithospermum erythrorhizon*

**(Graduate School of Agriculture,
Laboratory of Plant Gene Expression, RISH, Kyoto University)**

Kenta Kaminade

Shikonin, a red naphthoquinone pigment, is a plant specialized metabolite occurring only in some restricted species in Boraginaceae. A representative species is *Lithospermum erythrorhizon*, a medicinal plant growing in Japan, Korea and China. In this perennial herbal plant, shikonin deriveatives are specifically accumulated at the root bark. The name shikonin is derived from the Japanese name of the root 'shikon' that has been used as a crude drug in Asian countries for treatments of wounds, burns and hemorrhoids. *L. erythrorhizon* is, however, on the brink of extinction due to the environmental changes and indiscriminate harvesting.

On those backgrounds, cell suspension cultures of this plant capable of producing a large amount of shikonin derivatives were established in 1970s by the working group of the late Professor Mamoru Tabata, and the cell cultures were utilized for industrial production of shikonin by Mitsui Petrochemical Industries in 1980s [1]. The key point of this success is the establishment of shikonin production medium M9 [2], and the application of two-stage cultivation method with plant growth medium and pigment production medium, which enabled a large production rate of this plant specialized metabolite in cell suspension cultures. By this method almost the same composition of shikonin derivatives, which are esters of low molecular weight organic acids like acetate, could be produced.

We have been interested in understanding the biosynthetic rout of shikonin and its characteristic secretion mechanism, as these red lipophilic pigments are accumulated as a large number of red granules and oil droplets at the cell surface. In order to get an inventory of genes involved in the production of shikonin, we carried out transcriptome analysis using RNA-Seq of next generation sequencer. To narrow down the genes specifically expressed under shikonin production, we prepared three sets of RNA samples from shikonin-producing and non-producing tissues/cells: dark- and light-growing cell cultures, the same set of hairy root cultures, and root bark and peeled root, respectively.

As the results, we obtained ca. 254,000 reads, from which genes expressed more than three times higher under shikonin-producing tissues/cells than non-producing ones were picked up. Out of them, ca. 250 genes were up-regulated commonly under three independent tissues/cells, which were listed as triple positive genes. After cutting redundancy, 143 non-redundant genes were obtained, which were then classified according to the predicted functions, such as oxidoreductases, isomerases lyases, etc. Then, we will establish an evaluating system of those genes validating the relevance for shikonin biosynthesis and secretion.

Acknowledgements

I thank Dr. Hirobumi Yamamoto and Dr. Koichiro Shimomura of Toyo University for providing the *Lithospermum* cell line and shoot cultures, respectively. We also thank Dr. Tsuyoshi Nakagawa of Shimane University for the Gateway vector pGWB3 for plant expression.

References

[1] Fujita, Y., Tabata, M., Nishi, A., Yamada Y., "New medium and production of secondary compounds with the two-stage culture method" In: Plant Tissue Culture 1982. Fujiwara A (ed), pp. 312-313. Maruzen, 1982

[2] Fujita Y, Hara Y, Suga C, and Morimoto T. "Production of shikonin derivatives by cell suspension cultures of *Lithospermum erythrorhizon*. 2. A new medium for the production of shikonin deivatives" *Plant Cell Rep.* vol. 1, pp. 61-63, 1981.

ABSTRACTS (MASTER THESIS)

Functional analysis of a new sugar transporter in the nodule of *Lotus japonicus*

**(Graduate School of Agriculture,
Laboratory of Plant Gene Expression, RISH, Kyoto University)**

Mayuko Yoshimizu

Biological nitrogen fixation contributes largely to the global nitrogen cycle on the earth. In particular, symbiotic nitrogen fixation in legumes takes place in specialized organs called nodules. In infected plant cells of nodules, *Rhizobium* exists as bacteroids that are capable of reducing atmospheric N_2 to NH_3 and supplying the fixed nitrogen to the host plant. In turn, host plant provides photosynthetic metabolites as carbon source in forms of dicarboxylates. Beside, inorganic compounds that are required for the function of bacteroids are also transported across the membrane in nodule. In this process, various transporters should be involved at different membrane systems; however, little is known about the flow of carbon source from the plant cell to the symbiotic bacteria at the molecular level.

SWEET family is a sugar transporter family that was first identified in *Arabidopsis*. The fist member, AtSWEET1, is a facilitator protein involved in the excretion of monosaccharides such as glucose from plant cells [1]. Thereafter, other SWEET members have been found, which can transport sucrose in Arabidopsis and *Oryza sativa* [2, 3]. The family size of SWEET transporters is much smaller than other sugar transporter families reported previously.

In this study, we analyzed a member of SWEET transporter family of *Lotus japonicus* in order to gain an insight into the molecular mechanisms of the carbon transport from plant cells to bacteroids. In *L. japonicas* genome, thirteen members of SWEET family are found. Out of them, *LjSWEET3* was the only member that was highly expressed in the nodules. *LjSWEET3* expression was increased in accordance with the nodule development, and it reached the highest level in the mature nodule. Histochemical analysis using *L. japonicus* plants transformed with *LjSWEET3 promoter:GUS* showed the strong expression of this gene at the vascular systems in nodules. LjSWEET3-GFP fusion protein was expressed in the protoplasts of *Nicotiana banthamiana* and those of *Coptis japonica* to show its intracellular localization, demonstrating that the localization of LjSWEET3 was to be at the plasma membrane. The study is in progress by characterizing the RNAi mutants, and analyzing the relation of the gene with arbuscular mycorrhizal fungi.

Acknowledgements

This work is done as collaboration with Prof. Wolf B Frommer and Dr. Davide Sosso of Carnegie Institution in United States.

References

[1] Chen, L. C. et al. (2010). Sugar transporters for intercellular exchange and nutrition of pathogens. *Nature, 468*(7323), 527.

[2] Chen, L. C. et al. (2012). Sucrose efflux mediated by SWEET proteins as a key step for phloem transport. *Science, 335*(6065), 207-211.

[3] Yuan, M. Y. and Wang, S. W. (2013). Rice MtN3/Saliva/SWEET Family Genes and Their Homologs in Cellular Organisms. *Molecular Plant,* 6 (3), 665–674.

ABSTRACTS (MASTER THESIS)

Development of a 266 nm Raman lidar for profiling atmospheric water vapor

**(Graduate School of Informatics,
Laboratory of Atmospheric Sensing and Diagnosis, RISH, Kyoto University)**

Takuma UESUGI

It is projected that localized extreme weather events could increase due to the effects of global warming, resulting in severe weather disasters. Understanding water vapor's behavior in the atmosphere is essential to understand a fundamental mechanism of these weather events. Therefore, continuous monitoring system to measure the atmospheric water vapor with good spatio-temporal resolution is required. We have developed several water vapor Raman lidar systems employing the laser wavelengths of 355 and 532 nm. However, the signal-to-noise ratio of the Raman lidar strongly depends on the sky background because of the detection of the weak inelastic scattering of light by molecules. Therefore, these systems were mainly used during nighttime.

Hence, we have newly developed a water vapor Raman lidar using a laser at a wavelength of 266 nm. This wavelength is in the ultraviolet range below 300 nm known as the "solar-blind" region, because practically all radiation at these wavelengths is absorbed by the ozone layer in the stratosphere. It has the advantage of having no daytime solar background radiation in the system. The lidar is used for measuring the light separated into an elastic backscatter signal and vibrational Raman signals of oxygen, nitrogen and water vapor at wavelengths of 266, 277, 284, and 295 nm, respectively. This system can be used for continuous water vapor measurements in the lower troposphere.

We have demonstrated the potential of the 266nm Raman lidar at the middle and upper (MU) radar observatory in October 30-31, 2014. The mean values of standard deviation, which is differences of water vapor mixing ratio between the lidar and radiosonde, increased with height from 0.28 g/kg (up to 300 m) to 0.74 g/Kg (up to 600 m). The large values of the standard deviation at higher altitudes might be caused by the broken clouds which were observed above 400 m. We found a good agreement of the temporal variations of the water vapor mixing ratio near the ground between lidar and surface in-situ observations during experiment including the daytime.

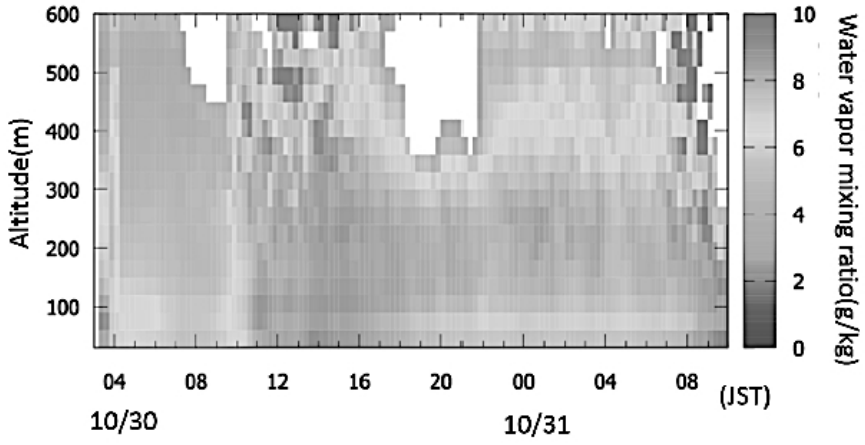

Figure 1. Temporal variation of vertical profiles of water vapor mixing ratio measured with the 266 nm Raman lidar at a middle and upper atmosphere (MU) radar site (34.9°N, 136.1°E, 385 m a.s.l.), Shigaraki, Japan, on October 30–31, 2014.

ABSTRACTS (MASTER THESIS)

Atmospheric dynamics in the mesosphere and lower thermosphere on the basis of long-term-radar observations

**(Graduate School of Geophysics,
Laboratory of Atmospheric Sensing and Diagnosis, RISH, Kyoto University)**

Naoki MATSUMOTO

In order to clarify the generation mechanism of the periodic oscillations of wind velocity and their irregular variations in an altitude range of 70-110 km in the equatorial Mesosphere and Lower Thermosphere (MLT) region, we analyzed the long-term observation data obtained from the meteor/MF radars in the Asia-Oceania region. Especially, in this study, we focused on a specific phenomenon called Mesospheric Quasi-Biannual Enhancement (MQBE). The MQBE phenomenon shows an enhancement of the westward wind in March equinox with an interval of 2-3 years. If we assume that the MQBE phenomenon is an enhancement of the westward phase of the Mesospheric Semiannual Oscillation (MSAO), the MQBE phenomenon should occur also in September equinox, but this phenomenon is not actually observed in September equinox. Therefore, another process which produces one-year periodicity of wind perturbations can be thought in addition to the generation mechanism of the MSAO phenomenon; however, the mechanism remains unknown. In this study, we examined two processes: (1) coupling of the meridional wind with an annual variation, and (2) seasonal variation of the atmospheric wave activity that produces the MQBE phenomenon.

Correlation analysis between the zonal and meridional winds

In the equatorial MLT region, the meridional wind flows from the summer to winter hemisphere with an annual period (Annual Oscillation: AO), so we can consider that the wind perturbations with an annual period should appear in the zonal component due to some coupling processes between the zonal and meridional winds. However, since the Coriolis force disappears on the equator, it is theoretically expected that the zonal wind does not interfere with the meridional wind at all. Here, we examined whether the correlation between the zonal and meridional winds can be recognized by analyzing the long-term wind data obtained from the MF radar at Tirunelveli. As a result, the long-term variation of the amplitude of SAO and AO as seen in the zonal and meridional winds, respectively, resembled each other. However, we could not statistically find a crucial evidence on this relationship.

Generation process of MQBE through atmospheric gravity waves

Rao et al. [2012] reported that an enhancement of atmospheric gravity wave activity in the equatorial MLT region tends to coincide with an occurrence of MQBE. This result suggests that atmospheric gravity waves produce the MQBE phenomenon. However, in order to clarify the relationship between the gravity wave activity and MQBE occurrence, the correlation analysis between the mean zonal wind and its variance is insufficient, and we need to obtain the momentum flux associated with atmospheric gravity waves. In this study, we adopted the Hocking method [Hocking, 2005] to determine the momentum flux from the radial wind velocity observed with the meteor wind radars at Koto Tabang and Biak. Since these two meteor wind radars having the same observation system are installed at two sites in Indonesia with a longitudinal distance of 4000 km, we can evaluate the momentum fluxes derived from the Hocking method by comparing the analysis results between at Koto Tabang and Biak. As a result, the variations of the momentum flux at Koto Tabang and Biak resemble each other during two periods (2011/12-2012/04 and 2013/06-2013/10) when both the data rates are relative large. Therefore, it can be concluded that we derived the momentum flux with high accuracy by adopting the Hocking method. Moreover, using the long-term observation data obtained from the meteor wind radar at Koto Tabang, we investigated the climatology of the zonal momentum flux within an altitude range from 86 to 94 km. As a result, the zonal momentum flux showed a semi-annual oscillation indicating that the maxima appear on February and August.

ABSTRACTS (MASTER THESIS)

Characteristics of tropical convection from a coordinated observation campaign in Indonesia

**(Graduate School of Science,
Laboratory of Atmospheric Sensing and Diagnosis, RISH, Kyoto University)**

Takafumi MATSUDA

A coordinated observation campaign was carried out using an X-band Doppler radar, GNSS (Global Navigation Satellite System) receiver network, balloon sonde, and AWS (Automatic Weather Station) from January to March 2013 in the Bandung basin, West Java. Although Bandung is situated at an altitude of about 700 m and surrounded by mountains with summits elevated over 1500 m above sea level, moist convections frequently take place within the basin. The objective of this study is to investigate the mechanisms of deep moist convection and moisture supply in Bandung by analyzing the observation data as well as referring to high resolution numerical model data simulated by Japan Meteorological Agency Non-hydrostatic Model (JMANHM).

Satellite cloud images showed that convections occurred around mountain slopes of Bandung almost every day during the coordinated campaign and the X-band radar data showed that cumulonimbi as tall as 15 km altitude were observed almost every day that cloud reach tropopause. In addition, clear diurnal variations of GNSS-derived PWVs (Precipital Water Vapor) were observed in many days during the campaign. We conducted detailed analysis about the case on 16 March 2013, in which large diurnal variations of PWVs and torrential rainfall inside the basin were observed (Figure 1). The points we want to clarify in this analysis were “cause of the diurnal variations of PWVs” and “mechanisms of convection initiation”.

As a result, it was found that moist air originated from the Indian Ocean was intruded into Bandung from the western basin (Figure 2), resulting in the large diurnal variations of PWVs. The convections inside the basin were initiated by low-level wind convergence at the southern basin. In addition, there was also a convection initiated by topographical forcing of moist air from the Indian Ocean at a mountain slope outside the basin. A sensitivity experiment using 10 times lower model topography showed largely different time variations of PWVs and rainfall distributions. These results suggest that, complicated topography of Bandung strongly influences on the diurnal variations of PWVs, the convection initiations and the rainfall distributions inside the basin.

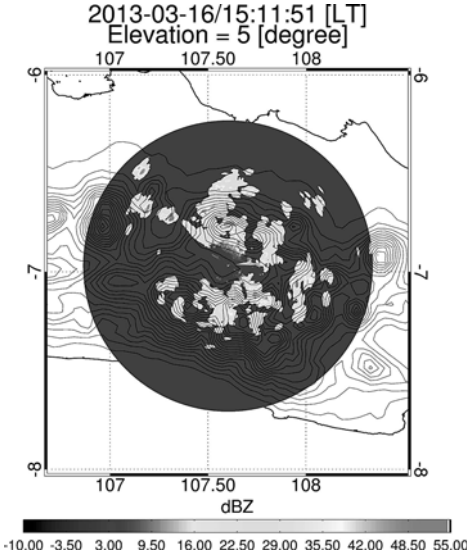

Figure 1. Map of radar refractivity at 1511 LT on 16 March 2013 observed by X-band radar.

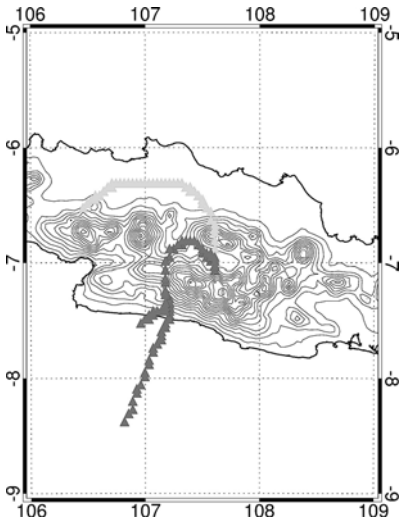

Figure 2. Trajectories of moist air parcels from 0800 LT to 1600LT on 16 March 2013.

ABSTRACTS (MASTER THESIS)

Development of rotational Raman lidar with a multispectral detector for profiling atmospheric temperature

**(Graduate School of Informatics,
Laboratory of Atmospheric Sensing and Diagnosis, RISH, Kyoto University)**

Kenichi YOSHIKAWA

Temperature profiling in the atmosphere is essential for studying atmospheric processes such as thermodynamics and cloud physics. Rotational Raman (RR) lidar can conduct continuous observation of the spatial distribution of atmospheric temperature. In this study, we developed a temperature lidar with a multispectral detector (MSD) in order to construct a system that is compact, robust, and easy to align for the detection of RR signals.

The spectral detection component of the temperature lidar consists of a grating and a photomultiplier (PMT) tube array with 32 channels. To remove the leakage effect caused by strong elastic scattering in the detector, we attempted two methods. First, we covered one PMT cathode strip of the elastic scattering channel to reduce the crosstalk effect. Second, we blocked the major portion of elastic scattering with the polarization beam splitter by using the polarization properties for spherical particles. The ideal settings for multispectral observations were determined by the theoretical simulation of accurate temperature projection based on the effects of both spectral resolution and spectral range, which influence the statistical error in temperature values of the lidar signals.

We constructed the temperature lidar with an MSD with 0.5nm spectral resolution at a laser wavelength of 532 nm. Simultaneous measurements with the proposed RR lidar and radiosonde were conducted at the middle and upper (MU) radar observatory in Shigaraki, Japan under clear sky conditions on the nights of November 5–8, 2013. The difference in photon detection efficiency at each MSD channel was calibrated using the radiosonde data. We found good agreement between the temperature profiles in the free troposphere between the lidar and radiosonde observations when both stokes branch (528.65 nm–531.65 nm) and anti-stokes branch (533.15 nm–536.15 nm) of RR lidar signals were used. The statistical error of the temperature values with an observation time of 4 h and a height resolution of 800m was 1.1K at an altitude of 7 km.

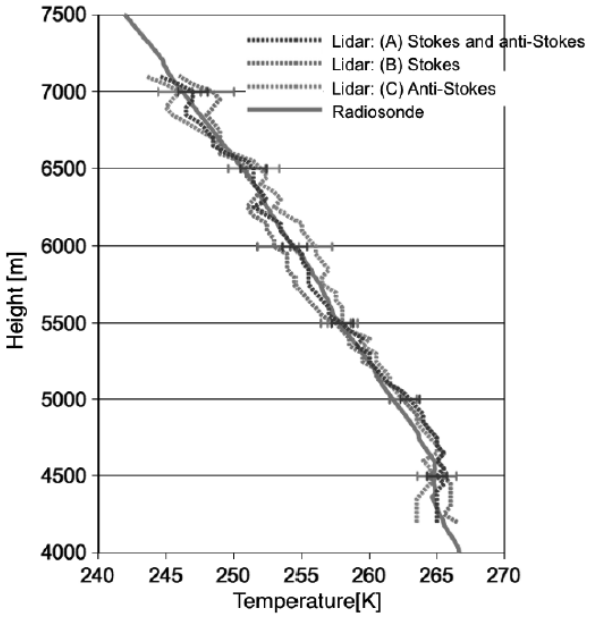

Figure 1. Temperature profiles measured with the rotational Raman (RR) lidar on 5 November 2013, 19:32 - 23:31 Japan standard time (JST). Radiosonde data at 20:29 JST is shown for comparison. Lidar data were smoothed with sliding average length 800 m. Error bars show the 1-σ statistical uncertainty of the RR temperature measurements using the photon-counting signals. The temperature retrievals were applied for the observed RR signals for three data types: (A) both Stokes and anti-Stokes lines, (B) Stokes lines, and (C) anti-Stokes lines.

ABSTRACTS (MASTER THESIS)

Aerosol Size Distribution Determined from Multiple Filed-Of-View Lidar

**(Graduate School of Informatics,
Laboratory of Atmospheric Sensing and Diagnosis, RISH, Kyoto University)**

Yutong LIU

Atmospheric aerosols play a key role in climate, air quality, and public health. Knowledge of aerosol size distribution is essential for determining its optical properties, cloud condensation nucleus activity, and physical activity related to particle deposition patterns in human lungs. Optical remote sensing techniques such as lidar are effective for monitoring aerosols with high temporal and spatial variation. Aerosol instruments using light with UV, VIS, and near-IR wavelengths have been used to effectively detect particles with diameters comparable to their wavelength. However, to quantitatively estimate the particle size distribution, more information of small particles with sub-micrometer size and below is required.

Conventional lidars employ a very small field-of-view (FOV) for profiling aerosol distribution and simply detect single scattering in the direction opposite to incident light, while multiple scattered signals are also influenced by aerosols' size and distribution along the laser path. In this study, a multiple FOV lidar with laser wavelengths of 266 and 355nm was used for detecting multiple scattering effects, in order to obtain more quantitative information concerning small particle size distribution. Although shorter wavelengths can be used for obtaining information of smaller particles, they have not been used for aerosol measurement owing to the strong light absorption by atmospheric constituents such as ozone.

Numerical simulation and field experiments were performed to verify the proposed method utilizing wavelengths of 532 and 1064nm for single scattering and 266 or 355nm for multiple scattering. In the simulation and field experiments, the multiple-scattering lidar observations at both wavelengths of 266 and 355nm supported the feasibility of proposed method. However, the 266nm lidar performed better than the 355nm lidar in the particle diameter range below 100 nm. We also found that the 266nm lidar can be applied to measurements under low particle concentration due to stronger multiple scattering.

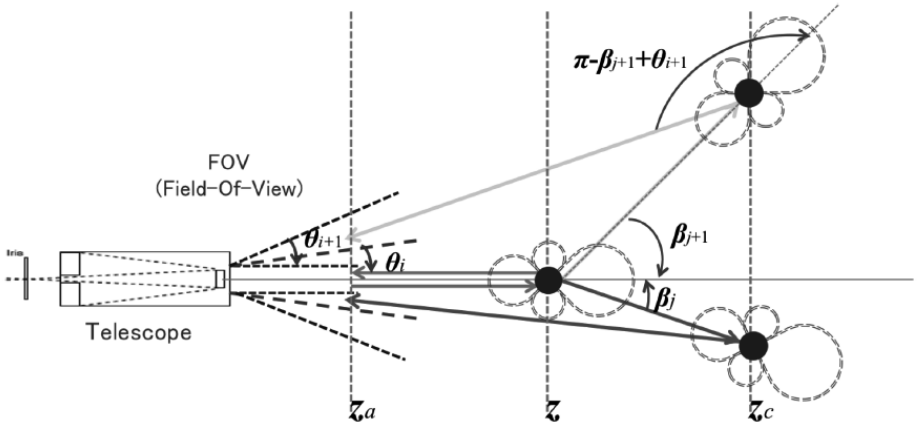

Figure 1. Schematic diagram of single scattering and multiple scattering in the lidar geometry. The straight arrows are the scattering events; the two pairs of dot lines indicate the limits of two receiver field of view that correspond to a narrow one for near-single-scattering detection and a wider one for multiple-scattering detection. Parameters of θ, z_c–z_a, and β are Field-Of-View(FOV), Aerosol layer thickness, and scattering angle, respectively.

ABSTRACTS (MASTER THESIS)

A Study on the development of forecast system for the downstream wind by Hira Oroshi

**(Graduate School of Informatics,
Laboratory of Radar Atmospheric Science, RISH, Kyoto University)**

Hiroto SAKAMOTO

This study aims to develop the precise forecast system of “Hira Oroshi" (hereafter, called as HO), the downstream gust wind blowing down from the Hira mountain range to the West coast of Biwa Lake in Shiga prefecture, Japan. Our system improved the forecast score of gust occurrence to about 80% from 50%. In this thesis, the occurrence of downstream gust wind in HO region is defined as the maximum wind speed exceeds to 20 m/s with the wind direction of WEW-NNE.

The intensive observation network was constructed to monitor the detailed behavior of downstream gust and selected four observation points, which can represent the wind field in the whole HO region. The non-hydrostatic meteorological forecast system with the horizontal resolution of 200 m is constructed by installing WRF (Weather Research and Forecast) to the A-KDK system in Kyoto University. The initial and boundary data is automatically obtained from JMA and other meteorological agencies every six hours. A long-term computational experiment from October 1, 2013 to March 31, 2014 shows very interesting characteristics of wind speed pattern, which appears, only when the gust wind was actually observed.

Narrow strong wind region extending from the Lake Biwa toward the foot of Hira mountain range appears and extends to the land in HO region. This structure is used to identify the appearance of gust wind in HO region. The threshold of strong wind in the forecast model is defined as 14 m/s in this study by considering the model wind velocity represents the averaged wind speed in horizontal grid and integral period. The new method by using this threshold shows very good forecast performance of hit ratio of about 80%. A performance of time series forecast was investigated. The forecast predicts longer gust wind period than the actual observation. A potential of the precise time series forecast is expected by adjusting the threshold.

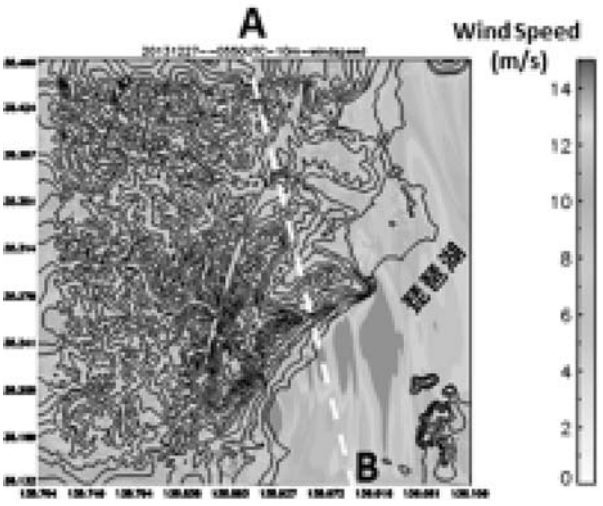

Fig.1 Surface wind speed simulated by numerical weather model.

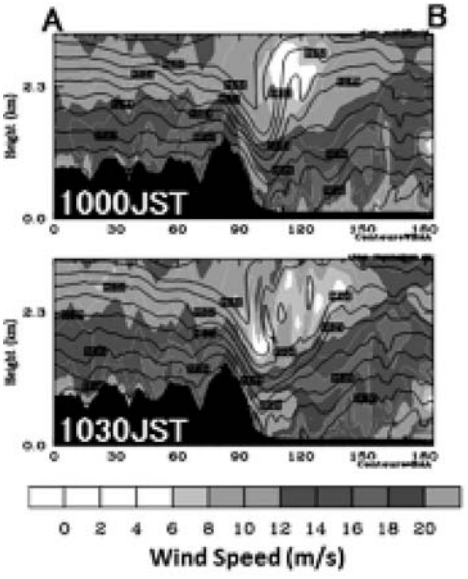

Fig.2 Vertical cross section of wind speed from A to B in Fig.1.

ABSTRACTS (MASTER THESIS)

Reinforcement of polypropylene with surface modified cellulose nanofiber

**Graduate School of Forest and Biomaterials science,
Laboratory of Active Bio-based Matesials, RISH, Kyoto University**

Yuka Kitano

Introduction

In order to reinforce polypropylene (PP) with cellulose nanofiber (CNF), it is effective to introduce hydrophobic functional groups on the surface of CNF. In this work, we chose eight types of functional groups (Figure 1). Each functional group was introduced on the surface of CNF by esterification. Chemically modified CNF/PP composites were prepared, and mechanical properties of these composites were evaluated.

Experimental

Preparation of surface modified CNF: Bacterial cellulose (Fujicco Co., Ltd.) was disintegrated by blender. After wash and solvent exchange, functional group was introduced on the surface of CNF by esterification(Fig. 1). The progress of reaction was determined by elemental analysis and FT-IR. The dispersibilities of the CNF samples in cyclohexane was tested.

Preparation of CNF/PP composite: Chemically modified CNF /PP (Japan Polypropylene Co.) composites (fiber content:5 wt %) were prepared by hot press(170℃). Mechanical properties of these composites were evaluated by tensile tests.

Results and discussion

Preparation of surface modified CNF: The FT-IR spectra of the CNF samples showed the typical signals of the ether groups. The degree of substitution was 0.15. CNF sample 1,2,4,8 in cyclohexane (solubility parameter δ 8.21, PP: δ 8.31) showed good dispersibilities of CNF.

Mechanical properties of CNF/PP composite: The results of tensile tests showed Table 1. The modulus of Film 1 is higher than Film 2, whereas dispersibilities of CNF in both composites was similar. This is because that blanched chain improved the interaction between filler and matrix. The modulus of Film 4 is almost same as that of Film 2. The modulus of Film 7 is lower than those of Film 2,4, because naphthalene is so incompatible with PP that the dispersibility of CNF was low. In order to get good dispersibilities of CNF, PP-like chain is necessary (Film 8). Therefore, the mechanical properties of the composite were efficiently enhanced by PP-like functional groups, which allowed good dispersibilities of CNF in the PP matrix and strong interactions between CNF and PP matrix.

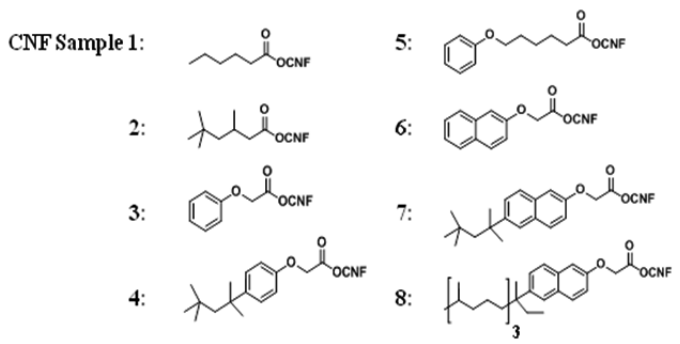

Figure 1. Eight surface modified CNFs

Table 1. The results of tensile tests

Film	Modulus [GPa]
Film 1 : CNF Sample 1/PP	2.42
2 : 2/PP	3.14
3 : 3/PP	2.91
4 : 4/PP	3.17
5 : 5/PP	2.19
6 : 6/PP	2.40
7 : 7/PP	2.82
8 : 8/PP	3.13
9 : PP	2.08

ABSTRACTS (MASTER THESIS)

Analysis of generation mechanism of geomagnetically induced current using the FDTD method

**(Graduate School of Electrical Engineering,
Laboratory of Space Radio Science Simulation, RISH, Kyoto University)**
Aoi Kimura

Geomagnetically induced currents (GIC) are known to flow in electric power transmission lines. GIC is induced by the ionospheric and magnetospheric currents, so that the GIC is a risk to power transmission system at high latitude where auroral electrojets flow in the ionosphere. The magnitude of GIC is small at middle and low latitude, and had been thought to be safe until the discovery that Sun-like stars can cause an extremely large solar flare, called a super flare. A possible impact of the solar flare on the Earth environment is fully unknown. To assess the risk for GIC in Japan, we need to understand the generation mechanisms of the ionospheric current and GIC. For the first step, we focused on GIC under the non-uniform electrical characteristics. The magnitude of the GIC depends on electrical characteristics under the ground, and the electrical characteristics are complicated under the Japan islands. It is still unclear the quantitative relationship between the ionospheric current and GIC under the complicated electrical characteristics. The purpose of this study is to investigate the generation mechanism of GIC and dependence on geographical characteristics by using the finite difference time domain (FDTD) method. First, we simulated the GIC in the case that the permittivity, conductivity and permeability depend on horizontal distance and depth (Figure 1). Our simulation result showed that the non-uniformity in the horizontal direction leads to the deviation of the charge at the discontinuity (Figure 2), and difference in the horizontal current (Figure 3). In contrast, the non-uniformity in the vertical direction leads to phase difference of the current. Secondly, we simulated the GIC in some realistic geometrical models, including an island model, a peninsula model, and a lake model. In these models, we gave the permittivity, conductivity and permeability in accordance with water and ground in the 3-dimensional space. In these cases, the charge tends to be accumulated at the discontinuity, resulting in the large electric field at the boundary (Figure 4).

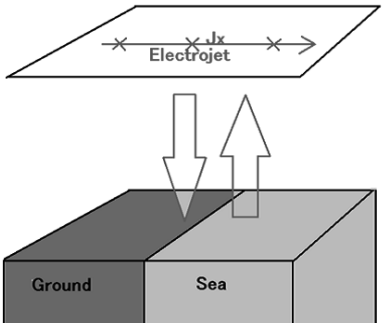

Figure 1. An example of a model depending on the horizontal direction.

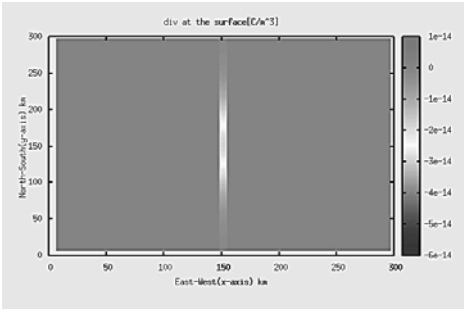

Figure 2. Accumulated charge.

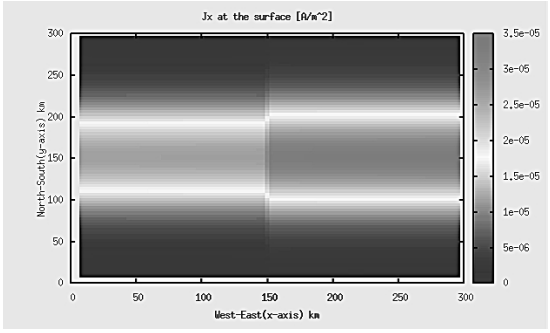

Figure 3. Current density flowing at the surface.

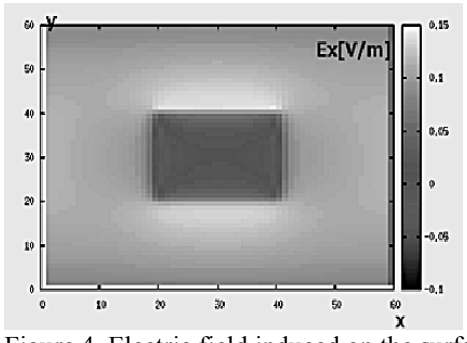

Figure 4. Electric field induced on the surface.

ABSTRACTS (MASTER THESIS)

Relativistic electron precipitation induced by EMIC triggered emissions in the Earth's magnetosphere

(Graduate School of Engineering, Laboratory of Computer Simulation for Humanospheric Sciences, RISH, Kyoto University)

Yuko Kubota

We perform test particle simulations of relativistic electrons [1] interacting with electromagnetic ion cyclotron (EMIC)-triggered emissions in the plasmasphere. EMIC-triggered emissions are generated by energetic protons injected into the inner magnetosphere. EMIC-triggered emissions are characterized by large wave amplitudes, rising-tone frequencies, and coherent left-hand circularly polarized waves [2]. We study trajectories of relativistic radiation belt electrons drifting eastward interacting with longitudinally distributed EMIC-triggered emissions. Some electrons are trapped by wave potentials and efficiently guided down to lower pitch angles [3]. Repeated interactions occur due to the mirror motion and result in the scattering of particles into the loss cone [4]. We use two EMIC wave models for the test particle simulations. One assumes that the wave amplitude is constant, and the other assumes a time-dependent wave amplitude that characterizes subpackets. Both model waves are resonant with 0.5–6.0 MeV electrons and precipitate them. Electrons in the energy range 1.1–3.0 MeV are precipitated most efficiently. Approximately 50% of the total injected number of 1.1–3.0 MeV electrons are precipitated in a timescale of 2 min. We obtain the relativistic electron distribution in equatorial pitch angle and in pitch angle at the atmosphere. Further, we determine the timing and longitudinal location of the relativistic electron precipitation with respect to different particle energies.

References

[1] Kubota, Y., Y. Omura, and D. Summers (2015), Relativistic electron precipitation induced by EMIC-triggered emissions in a dipole magnetosphere, J. Geophys. Res. Space Physics, 120, 4384–4399, doi:10.1002/2015JA021017.

[2] Omura, Y., J. S. Pickett, B. Grison, O. Santolik, I. Dandouras, M. Engebretson, P. M. E. Decreau, A. Masson (2010), Theory and observation of electromagnetic ion cyclotron triggered emissions in the magnetosphere, J. Geophys. Res., 115, A07234, doi:10.1029/2010JA015300.

[3] Omura, Y., and Q. Zhao (2012), Nonlinear pitch-angle scattering of relativistic electrons by EMIC waves in the inner magnetosphere, J. Geophys. Res., 117, A08227, doi:10.1029/2012JA017943.

[4] Omura, Y., and Q. Zhao (2013), Relativistic electron microbursts due to nonlinear pitch-angle scattering by EMIC triggered emissions, J. Geophys. Res., 118, 5008–5020, doi: 10.1002/jgra.50477.

ABSTRACTS (MASTER THESIS)

Study on an Auto Tracking Microwave Power Transmission System for a Mars Observation Airplane

(Graduate School of Engineering, Laboratory of Applied Radio Engineering for Humanosphere, RISH, Kyoto University)

Masashi Iwashimizu

In order to attain the weight saving of a Mars observation airplane, we are planning to supply energy by microwave. This paper presents auto tracking, which is composed of direction detection and beam direction control. First, we estimated the system requirements of the transmission system. Second, we described phase control of a magnetron, and an image processing method. With them, we conducted ground flight experiments, and succeeded in flying an airplane by an auto tracking microwave power transmission system. However, the direction detection error of the image processing method and its calculation time is larger than the requirements. In order to meet requirements, we adopted the method using pilot signal. By acquiring phase difference of receiving antennas, we calculate the direction of the airplane. For weight saving, we utilize second harmonics radiated from the rectennas mounted on the airplane as pilot signal. Third, we measured the power of the second harmonics radiated from the rectifying circuit we used in ground experiments, and found that the generated second harmonics power was weaker than the input microwave power by 20 dB. Forth, we described phase difference detection circuits, especially an amplifier circuit and a quadrature detection circuit. We used automatic gain control in order to input the constant amplitude into the quadrature detection circuit. We also used a feedback loop in the 90 ◦ phase shifter circuit to improve the accuracy of phase shift. Finally, we conducted direction detection experiments utilizing the second harmonics radiated from 15 rectennas mounted on a ground experiment airplane, and made out that the rectennas composed a phased array. If pilot signal is radiated from a phased array, its phase differs as the direction changes and causes phase difference error on the direction detection antennas. When this phased array directs its main lobe to the direction detection antennas, this phenomenon causes less effect. Therefore, if we can control the phase of the second harmonics from rectennas, we can adopt this method in Mars observation.

Acknowledgements

Part of this research was carried out by use of Microwave Energy Transmission Laboratory (METLAB) as collaborative inter-university research facility and was carried out with Kyosyu Institute of Technology.

ABSTRACTS (MASTER THESIS)

Study on a Transmission Antenna of a Demonstration Experiment Satellite for Solar Power Station

**(Graduate School of Engineering,
Laboratory of Applied Radio Engineering for Humanosphere, RISH, Kyoto University)**

Junki Yoshino

In this thesis, I study the requirements and performance of beam control for a satellite experiment to demonstrate wireless energy transfer technology on orbit for the purpose of Solar Power Satellite Station. Firstly, I show the requirements of the demonstration. In this demonstration, it is necessary to keep the beam direction accuracy within 0.2o I conducted practical experiments by using Advanced Phased Array System (APAS). I changed the beam direction from -30o to 30o, and measured the beam-direction errors. The error of beam-direction estimation became less than 0:055o with five-bits phase control. As the results, it is feasible to control the beam direction with an accuracy of 0:2o or less. Secondly, I evaluate the accuracy of the beam-direction estimation on the ground power receiving system. I show that the error of the beam-direction estimation is less than 0.1o on condition that the signal-to-noise ratio is limited -20 dB, with the least-square method and the spline interpolation. Thirdly, I propose a new method of reducing the side lobe only by controlling the phase of each antenna element. By controlling the phase of the adjacent pair antenna, the virtual power taper can be realized. I evaluate the performance of the proposed method, and it is shown that the side-lobe level is reduced to less than -30 dB by using this method. However, a directional gain depends on the types of taper distribution despite the same reduction level. Gauss distribution and Chebyshev distribution, and these distribution should be chosen properly according to the situation. I also investigate the real performance of the proposed method by some experiments. Although the side-lobe level in near field is higher than as expected, the proposed method reduce the side lobe effectively. The difference between experiments and the simulation results is caused by the misplacement of a receiving antenna, and the side-lobe level in far field is approximately the same with the simulations. Thus, the proposed method would be effective for reducing the side-lobe level in experiment. Finally, I show that the proposed method can be used for the satellite experiment.

Acknowledgements

Part of this research was carried out by use of Microwave Energy Transmission Laboratory (METLAB) as collaborative inter-university research facility and was supported by ISAS/JAXA.

ABSTRACTS (MASTER THESIS)

Development of a Broadband Small-size Electromagnetic Wave Irradiation Applicator for Microwave Chemical Reaction

**(Graduate School of Engineering,
Laboratory of Applied Radio Engineering for Humanosphere, RISH, Kyoto University)**

Ryo Nakajima

It is known that microwave-assisted chemical reaction has some advantages. Generally, 2.45 GHz microwave is used for microwave heating, on the other hand, the efficiency of dielectric heating depends on frequency. Thus, there is a possibility that microwave-assisted chemical reaction takes place more at any other frequency efficiently than 2.45 GHz. The objective of our research is to develop a broadband small-size electromagnetic wave irradiation applicator for microwave chemical reaction. First, we measured the permittivity of sodium hydroxide solution which is assumed as solvent of chemical reaction. We calculated the penetration depth and the microwave absorbing power of sodium hydroxide solution by using the data of the permittivity. Second, we designed a broadband small-size electromagnetic wave irradiation applicator by using an electromagnetic simulator. The heated product is assumed to be a 2 mol/L sodium hydroxide solution of 20 mL. We aim that the reflection coefficient is less than -10 dB in 0.08 GHz–2.7 GHz. We simulated the several sizes of applicators. In addition, we changed the applicator in consideration of manufacturing. The reflection coefficient of designed applicator was less than -10 dB in 0.42 GHz–0.63 GHz and 2.27 GHz–2.7 GHz. Third, we manufactured a broadband small-size electromagnetic wave irradiation applicator. We conducted reflection measurement and the experimental results are approximately consistent with the simulation results. Next, we conducted heating experiment by changing the frequency, and it is shown that the temperatures of the heated product rose to 100 degrees in 290 to 370 seconds. Then, we performed thermal analysis simulation and we compared the simulation result and the experimental result. Finally, we presented the temperature control experiment. We created LabVIEW programs and we made a comparison of P control, PI control and PID control.

Acknowledgements

Part of this research was supported by CREST, JST and carried out as collaborative research with Laboratory of Biomass Conversion, RISH, Kyoto University.

ABSTRACTS (MASTER THESIS)

Study on Space Debris Removal Using Geomagnetic Lorentz Force

**(Graduate School of Engineering,
Laboratory of Space Systems and Astronautics, RISH, Kyoto University)**

Yosuke Akashi

The purpose of this study is to propose new methods for space debris removal using geomagnetic Lorentz force. The Lorentz force is produced when a charged object moves through a magnetic field. In this study, we assume space debris can be charged using small electron emitter, and generate the Lorentz force with the interaction between the charged space debris and the Earth's magnetic field. Then, we actively control charge to mass ratio (CTMR) of the space debris using the emitter, and control its orbit by the Lorentz force, aiming to make the space debris reach the Earth's atmosphere. First, we applied constant CTMR of 0.03 C/kg to the space debris. In this case, we found it difficult to make space debris reach the earth's atmosphere, because the oscillation of the altitude of the space debris is no more than 3 meters. Thus, we investigated two method to enable the removal by ON/OFF control of the emitter.

The first method is the excitation method. In this method, we focus on the oscillation of the altitude and turn on the emitter when the Lorentz force excites the oscillation of the altitude. Using this method, the eccentricity of the orbit become larger and larger, and finally the perigee reaches the Earth's atmosphere. For example, if the space debris has the inclination of 98.6 degree and the altitude of 800 km initially, the space debris reaches the Earth in 25 days. However, this method is effective only when the initial inclination is 90 degree to 180 degree. Besides, if the space debris has initial altitude of 1,500 km or more, the oscillation of the altitude will converge.

The second method is the energy attenuation method. We turn on the emitter when the Lorentz force attenuates the energy (in other words, when the Lorentz force acts in the opposite direction of space debris' velocity). Using this method, the energy of space debris gradually decreases and the altitude of the space debris decreases monotonically, because the radius of the orbit depends on the energy. For example, if the space debris has the inclination of 98.6 degree and the altitude of 500 km initially, the space debris reaches the Earth in 75 days. However, this method is effective only when the initial inclination is 5 degree to 160 degree. Furthermore, because the inclination keeps increasing while charging, the reduction of the altitude will converge when the inclination reaches 160 degree.

ABSTRACTS (MASTER THESIS)

Study on Shape Estimation of Space Debris Using MU Radar

**(Graduate School of Engineering,
Laboratory of Space Systems and Astronautics, RISH, Kyoto University)**

Atsuhito Kawahara

It is widely known that regular observation of space debris in low earth orbit is one of the most important task for realization of sustainable space exploration. The aim of this study is to develop a method of estimating the shape of space debris with a ground-based station, the MU radar, which is not used for debris observation but for atmospheric observation because of low range resolution.

In previous study, Single Range Doppler Interferometry(SRDI) method was proposed, which can roughly image the shape of space debris using a fluctuating doppler spectrogram caused by the spin motion of space debris by means of numerical simulation [1]. Therefore, we examined the SRDI method by means of numerical simulation and observation. We used the pseudo wigner-ville distribution(PWVD) method to get a fluctuating doppler spectrogram which can be obtained from time-frequency analysis. In numerical simulation, space debris was expressed by many point targets and wire grid model. We confirm accuracy and validity of SRDI method. As a result of observation, the size of errors between the estimated size and the real size of space debris were within 0.5 m. As to the spacecraft adapter whose real diameter was 119.4 ~ 166.6 cm, we estimated its size at 40 ~ 140 cm.

In addition, We focused on Radar Cross Section(RCS) fluctuation. The RCS fluctuation of a perfectly conductive ellipsoid can be calculated analytically, so we assumed the debris to be an ellipsoid and fitted a curve to observed data in order to extract information about the shape of debris. By using this method, the spacecraft adapter already mentioned was estimated to be an elliptic plane whose major axis is 127 cm and minor axis is 98 cm. In this method, it is estimate that Spacecraft adapter whose diameter is 119.4 ~ 166.6 cm at elliptic plate whose major axis is 1.27 cm and minor axis is 0.98 cm. Moreover, taking this method together with the SRDI method made it possible to obtain not only information about the shape of debris but also the spin rate and the posture.

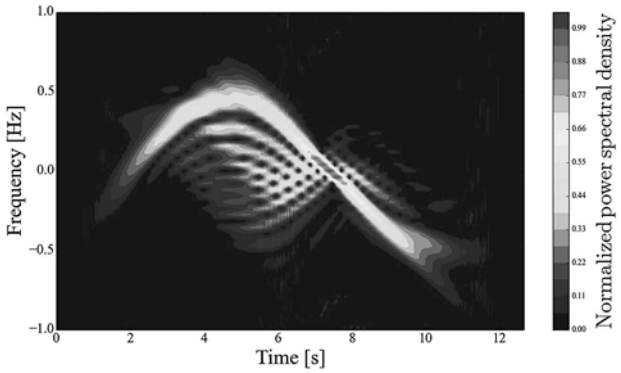

Figure 1. Calculation result of the time-frequency analysis of a space debris signal using PWVD

References

[1] T. Sato,, “Shape Estimation of Space Debris Using Single-Range Doppler In-terferometry”, *IEEE TGARS*, vol. 37., no.2, pp. 1000 -1005, 1999.

ABSTRACTS (MASTER THESIS)

Analysis of Active Spacecraft Charging in the Geostationary Environment

**(Graduate School of Engineering,
Laboratory of Space Systems and Astronautic, RISH, Kyoto University)**

Kento Hoshi

A new concept of spacecraft orbital control using electromagnetic forces such as the Lorentz force and the Coulomb force has been recently proposed. Spacecraft controls their orbit by controlling their potential using a charged-particle emitter. This control method may provide propellantless orbital control and a very lightweight propulsion system compared with conventional chemical and electric propulsion systems.

To control the electromagnetic force that acts on the spacecraft, it is necessary to actively control the spacecraft's electrical potential. The active spacecraft potential control method, however, has only been used to mitigate spacecraft charging, and little has been reported on active charging. For evaluating the performance and feasibility of electromagnetic orbital control, we reveal the electric potential characteristics of active spacecraft charging by using a 3-D full Particle-in-Cell (PIC) simulation.

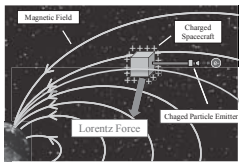

Figure 1. Artistic Image of Electromagnetic Orbital Control

Firstly, we improved an electrostatic spacecraft charging analysis code, called HiPIC, which was developed by the Japan Aerospace Exploration Agency's Engineering Digital Innovation Center. We implemented a beam-emission routine, applied OpenMP parallelization to the code, and adapted it for a multi-compiling.

Secondly, we performed the active spacecraft charging simulations. We defined a cubic spacecraft model and simulated electron beam emission from the surface.

As a result, we showed the simple beam-returning model cannot accurately express the electric potential characteristics of active spacecraft charging We assumed a boundary between ``beam-returning region'' and ``not beam-returning region'' can be determined as the point of background electric current becomes equal to electron beam current, and formularized the theoretical potential characteristics. It roughly agrees with the PIC simulation results, but it does not simulate the potential gradient in the beam-returning region.

Thirdly, we proposed a new active charging model. Our main concept is to modify the return current term in the conventional model. The electric potential of a cubic spacecraft can be numerically calculated with our model; by contrast, the conventional model can only expresses active charging qualitatively.

Finally, we evaluated the Lorentz force characteristics in the geostationary environment to evaluate performance and applications of electromagnetic orbital control. The Lorentz force is in proportion to the spacecraft's potential, so that the force also depends on the background plasma environment. A rod-shaped spacecraft can generate larger Lorentz force than a cubic spacecraft on the same surface area because a spacecraft's capacitance depends on the space shape.

ABSTRACTS (MASTER THESIS)

Development of the multiple-point observation system for space plasmas

(Graduate School of Engineering, Laboratory of Space Systems and Astronautic, RISH, Kyoto University)

Takahiro Zushi

Space is filled with dilute plasmas that are essentially collisionless. In collisionless plasmas, kinetic energies of particles are exchanged through wave-particle interactions. These waves are plasma waves. The observation of plasma waves in space is essential in monitoring the space electromagnetic environment, as well as for understanding physical processes taking place in space. Consequently, plasma waves have been observed in the past scientific missions that target the investigation of space plasmas phenomena.

Recently, the missions on the basis of multiple-point observations have become the trend since conventional one-point observations cannot distinguish between time and spatial variations. We propose a new system for multiple-point observation [1]. The system consists of sensor probes that can measure electromagnetic waves and transfer data to the central station through wireless communication. We developed the prototype model of the sensor probe, and we also developed the new miniaturized plasma wave receiver for sophistication of the sensor probe.

Prototype model of the small sensor probe

We developed the prototype model of the small sensor probe. The sensor probe include the plasma wave receiver, the microcontroller, the wireless communication module, electromagnetic sensors, and the battery in 130 mm cubic. Thus it has the ability to measure plasma waves and transfer observation data through wireless. Figure.1 shows a photograph of the sensor probe. We verified the total performance for electric field measurements, and we found that analog components had enough characteristics to measure electric fields, and the A/D conversion and the wireless transmission worked correctly. We also found that the sensitivity for electric field is -140 dBV/m $/\sqrt{\mathrm{Hz}}$. The sensitivity is sufficiently high to capture intense plasma wave such as electron cyclotron harmonic waves.

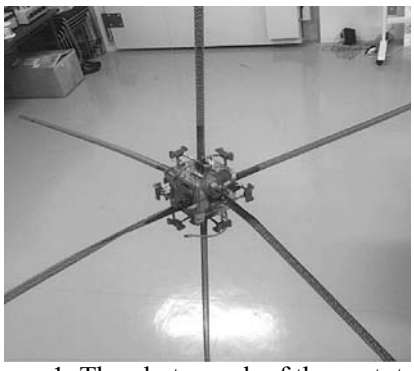

Figure 1. The photograph of the prototype model of the sensor probe.

Miniaturized spectrum plasma wave receiver

Plasma wave receivers are categorized into two types: waveform receiver and spectrum receiver. Present sensor probe measure waveform of plasma waves using waveform type of plasma wave receiver. Although the waveform receiver can provide phase data, it has disadvantages that it cannot measure continuously due to the data size of the waveform. Thus it is desirable to use both types of receivers in plasma wave observation.

We propose a new types of spectrum receiver that combine analog circuit and digital signal processing. The analog circuit of the receiver provide band-limited waveform of the plasma, and signal processor carry out Fast Fourier Transform to get detailed spectrum of the plasma wave. We developed the analog circuit of the new spectrum receiver by using ASIC (Application-Specific Integrated Circuits). We verified that the developed circuit can use for the new spectrum receiver.

References

[1] Kojima H, Fukuhara H, Mizuochi Y, Yagitani S, Ikeda H, Miyake Y, Usui H, Iwai H, Takizawa Y, Ueda Y, Yamakawa H "Miniaturization of plasma wave receivers onboard scientific satellites and its application to the sensor network system for monitoring the electromagnetic environments in space." *Advances in Geosciences.*, 21, 461-481, 2010.